Defense Nuclear Agency
Alexandria, VA 22310-3398

DNA-TR-92-10

Railgun Armature Velocity Improvement SBIR Phase II

Leo E. Thurmond
David P. Bauer
IAP Research, Inc.
2763 Culver Avenue
Dayton, OH 45429-3723

August 1992

Technical Report

CONTRACT No. DNA 001-90-C-0024

Approved for public release;
distribution is unlimited.

Destroy this report when it is no longer needed. Do not return to sender.

PLEASE NOTIFY THE DEFENSE NUCLEAR AGENCY, ATTN: CSTI, 6801 TELEGRAPH ROAD, ALEXANDRIA, VA 22310-3398, IF YOUR ADDRESS IS INCORRECT, IF YOU WISH IT DELETED FROM THE DISTRIBUTION LIST, OR IF THE ADDRESSEE IS NO LONGER EMPLOYED BY YOUR ORGANIZATION.

DISTRIBUTION LIST UPDATE

This mailer is provided to enable DNA to maintain current distribution lists for reports. (We would appreciate your providing the requested information.)

NOTE:
Please return the mailing label from the document so that any additions, changes, corrections or deletions can be made easily.

☐ Add the individual listed to your distribution list.

☐ Delete the cited organization/individual.

☐ Change of address.

NAME: _____

ORGANIZATION: _____

OLD ADDRESS	CURRENT ADDRESS
_____	_____
_____	_____
_____	_____

TELEPHONE NUMBER: ( ) _____

DNA PUBLICATION NUMBER/TITLE	CHANGES/DELETIONS/ADDITIONS, etc. *(Attach Sheet if more Space is Required)*
_____	_____
_____	_____
_____	_____

DNA OR OTHER GOVERNMENT CONTRACT NUMBER: _____

CERTIFICATION OF NEED-TO-KNOW BY GOVERNMENT SPONSOR (if other than DNA):

SPONSORING ORGANIZATION: _____

CONTRACTING OFFICER OR REPRESENTATIVE: _____

SIGNATURE: _____

FOLD HERE AND RETURN

DEFENSE NUCLEAR AGENCY
ATTN: TITL
6801 TELEGRAPH ROAD
ALEXANDRIA, VA 22310-3398

DEFENSE NUCLEAR AGENCY
ATTN: TITL
6801 TELEGRAPH ROAD
ALEXANDRIA, VA 22310-3398

REPORT DOCUMENTATION PAGE

Form Approved
OMB No. 0704-0188

1. AGENCY USE ONLY *(Leave blank)*	2. REPORT DATE	3. REPORT TYPE AND DATES COVERED
	920801	Technical 900301 - 911231

4. TITLE AND SUBTITLE
Railgun Armature Velocity Improvement SBIR Phase II

5. FUNDING NUMBERS
C-DNA 001-90-C-0024
PE - 62715H
PR - SF
TA - SB
WU - DH300840

6. AUTHOR(S)
Leo E. Thurmond and David P. Bauer

7. PERFORMING ORGANIZATION NAME(S) AND ADDRESS(ES)
IAP Research, Inc.
2763 Culver Avenue
Dayton, OH 45429-3723

8. PERFORMING ORGANIZATION REPORT NUMBER
IAP-TR-91-09

9. SPONSORING/MONITORING AGENCY NAME(S) AND ADDRESS(ES)
Defense Nuclear Agency
6801 Telegraph Road
Alexandria, VA 22310-3398
RAEV/Nichols

10. SPONSORING/MONITORING AGENCY REPORT NUMBER
DNA-TR-92-10

11. SUPPLEMENTARY NOTES
This work was sponsored by the Defense Nuclear Agency under RDT&E RMC Code B7664D SF SB 00072 PRPD 1950A 25904D. Additional support and funding provided by the Strategic Defense Initiative Office.

12a. DISTRIBUTION/AVAILABILITY STATEMENT
Approved for public release; distribution is unlimited.

12b. DISTRIBUTION CODE

13. ABSTRACT *(Maximum 200 words)*

Railgun hypervelocity performance has not been repeatably demonstrated at velocities over 6 km/s. A significant performance limiting phenomena is the formation of secondary current paths in parallel with the main projectile accelerating plasma.

A confined plasma armature technique was developed to prevent secondary armature formation.

Confinement prevents loss of ionized material from the plasma armature and thereby prevents formation of a low rail-to-rail conductance. We controlled pressure in the confined armature via controlled venting through ports in the rails.

Railgun tests with the confined armature show that sealing at the rail-confinement vessel interface is critical and difficult to achieve. Our tests show that during low seal leakage operation secondaries are prevented. However, maintaining good seal for the entire launch is very difficult.

14. SUBJECT TERMS
Plasma Armature
Confined Plasma Armature
Railgun Limit Velocity Improvement

15. NUMBER OF PAGES
68

16. PRICE CODE

17. SECURITY CLASSIFICATION OF REPORT	18. SECURITY CLASSIFICATION OF THIS PAGE	19. SECURITY CLASSIFICATION OF ABSTRACT	20. LIMITATION OF ABSTRACT
UNCLASSIFIED	UNCLASSIFIED	UNCLASSIFIED	SAR

CLASSIFIED BY:

N/A since Unclassified

DECLASSIFY ON:
N/A since Unclassified

CONVERSION TABLE

Conversion factors for U.S. customary to metric (SI) units of measurement

To Convert From	To	Multiply
angstrom	meters (m)	1.000 000 X E–10
atmosphere (normal)	kilo pascal (kPa)	1.013 25 X E+2
bar	kilo pascal (kPa)	1.000 000 X E+2
barn	meter^2 (m^2)	1.000 000 X E–28
British Thermal unit (thermochemical)	joule (J)	1.054 350 X E+3
calorie (thermochemical)	joule (J)	4.184 000
cal (thermochemical)/cm^2	mega joule/m^2(MJ/m^2)	4.184 000 X E–2
curie	giga becquerel (GBq)*	3.700 000 X E+1
degree (angle)	radian (rad)	1.745 329 X E–2
degree Fahrenheit	degree kelvin (K)	t_K=(t°f + 459.67)/1.8
electron volt	joule (J)	1.602 19 X E–19
erg	joule (J)	1.000 000 X E–7
erg/second	watt (W)	1.000 000 X E–7
foot	meter (m)	3.048 000 X E–1
foot–pound–force	joule (J)	1.355 818
gallon (U.S. liquid)	meter^3 (m^3)	3.785 412 X E–3
inch	meter (m)	2.540 000 X E–2
jerk	joule (J)	1.000 000 X E+9
joule/kilogram (J/Kg) (radiation dose absorbed)	Gray (Gy)	1.000 000
kilotons	terajoules	4.183
kip (1000 lbf)	newton (N)	4.448 222 X E+3
kip/inch^2 (ksi)	kilo pascal (kPa)	6.894 757 X E+3
ktap	newton–second/m^2 (N–s/m^2)	1.000 000 X E+2
micron	meter (m)	1.000 000 X E–6
mil	meter (m)	2.540 000 X E–5
mile (international)	meter (m)	1.609 344 X E+3
ounce	kilogram (kg)	2.834 952 X E–2
pound–force (lbf avoirdupois)	newton (N)	4.448 222
pound–force inch	newton–meter (N·m)	1.129 848 X E–1
pound–force/inch	newton/meter (N/m)	1.751 268 X E+2
pound–force/foot^2	kilo pascal (kPa)	4.788 026 X E–2
pound–force/inch^2 (psi)	kilo pascal (kPa)	6.894 757
pound–mass (lbm avoirdupois)	kilogram (kg)	4.535 924 X E–1
pound–mass–foot^2 (moment of inertia)	kilogram–meter^2 (kg·m^2)	4.214 011 X E–2
pound–mass/foot^3	kilogram/meter^3 (kg/m^3)	1.601 846 X E+1
rad (radiation dose absorbed)	Gray (Gy)**	1.000 000 X E–2
roentgen	coulomb/kilogram (C/kg)	2.579 760 X E–4
shake	second (s)	1.000 000 X E–8
slug	kilogram (kg)	1.459 390 X E+1
torr (mm Hg, 0°C)	kilo pascal (kPa)	1.333 22 X E–1

*The becquerel (Bq) is the SI unit of radioactivity; Bp = 1 event/s.

**The Gray (Gy) is the SI unit of absorbed radiation.

TABLE OF CONTENTS

LIST OF ILLUSTRATIONS

LIST OF ILLUSTRATIONS - CONT.

LIST OF TABLES

SECTION 1
INTRODUCTION

1.1 CONCEPT.

Our ultimate goal in this program was to develop an armature-barrel design capable of exceeding 6 km/s with a railgun projectile. This velocity represents a performance level to which plasma armatures have been taken, but only rarely exceeded.[1] Velocities greater than 6 km/s are impeded by secondary current conduction behind the armature. The plasma in the armature interacts with the insulators and rails in the bore, causing ablation of the wall materials. Some of the ablated material is ionized, so it is conductive. Drag forces combined with low Lorentz force near the insulators result in a loss of some of the conductive plasma from the armature. This residual conductive plasma is left in the bore behind the main armature. Secondary current conduction results because the rail-to-rail voltage tends to drive current through the lost plasma behind the armature. This situation is shown in Figure 1.

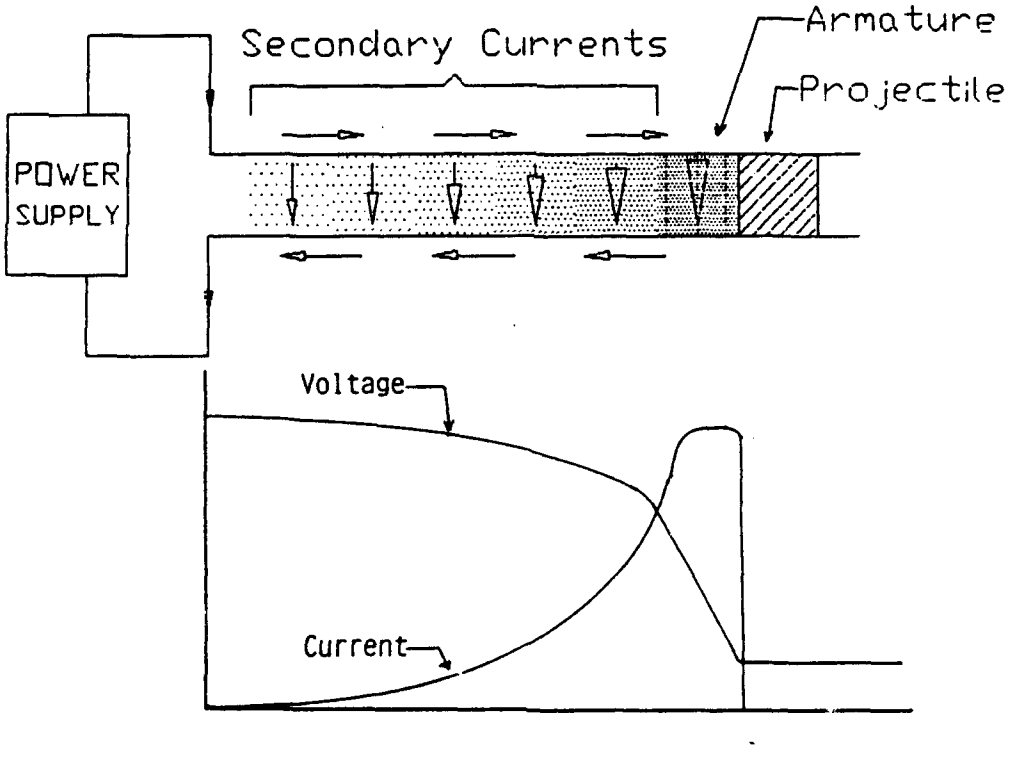

Figure 1. High voltage and leaking plasma result in secondary currents.

The interaction of the armature current with the magnetic field between the rails exerts a force on the armature. This force is transmitted to the projectile, and the projectile is accelerated. The secondary current conduction diverts the current from the main armature. This results in the armature being accelerated less than was theoretically predicted. The problem of secondary current conduction gets

worse at higher velocities. As the projectile goes faster, more current is diverted from the main armature into secondary current paths. This process continues until the projectile itself is no longer accelerated by the current.

There are two areas to attack in the solution of this problem. First, we can reduce or eliminate the rail-to-rail voltage behind the armature. We can do this by distributing the power feeds along the rails and only supplying current to the rail sections directly behind the armature. This is the idea behind distributed energy store (e.g. Nested Chevron DES[2] and Ultra DES[3]) railguns and SRS concept.[4]

The other area we can concentrate on is the residual plasma. We can approach this problem in two ways. We can reduce the conductivity of the residual plasma, or we can eliminate the plasma from behind the armature altogether. There are several ways to deal with the residual plasma.[1] These are shown in Figure 2. The approach we chose to pursue in this project was to try to eliminate the plasma from behind the armature by venting it out through the rails. This concept is shown in Figure 3. We developed the concept in a Phase I SBIR.[5] We will describe Phase II work on this concept in this report after a brief review of the Phase I results.

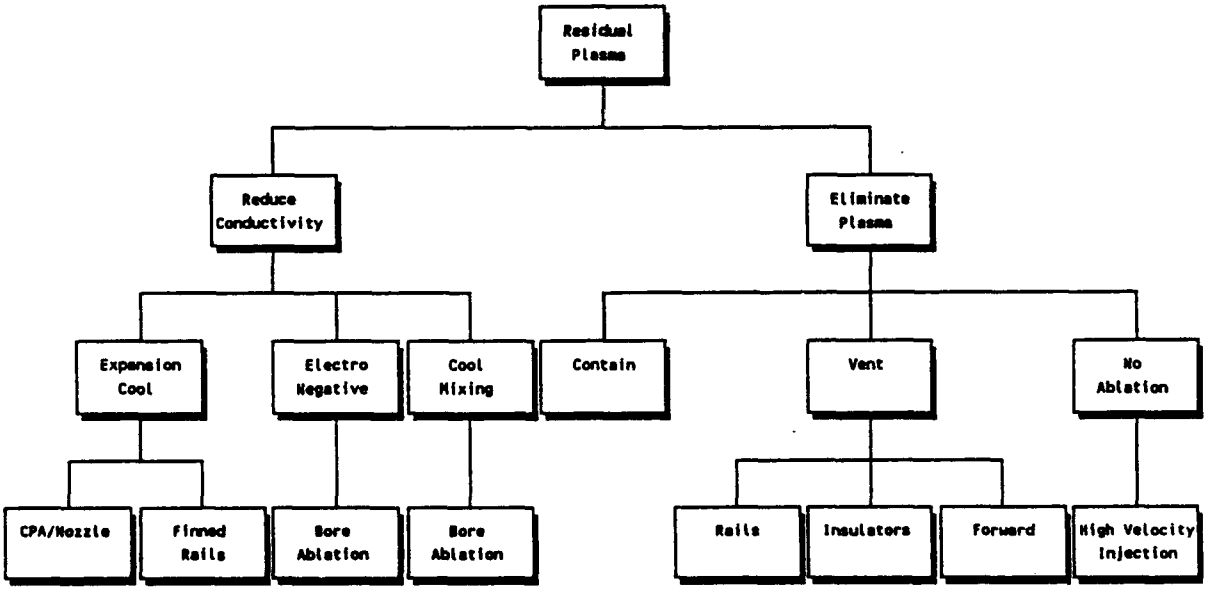

Figure 2. There are several methods to eliminate secondary currents.

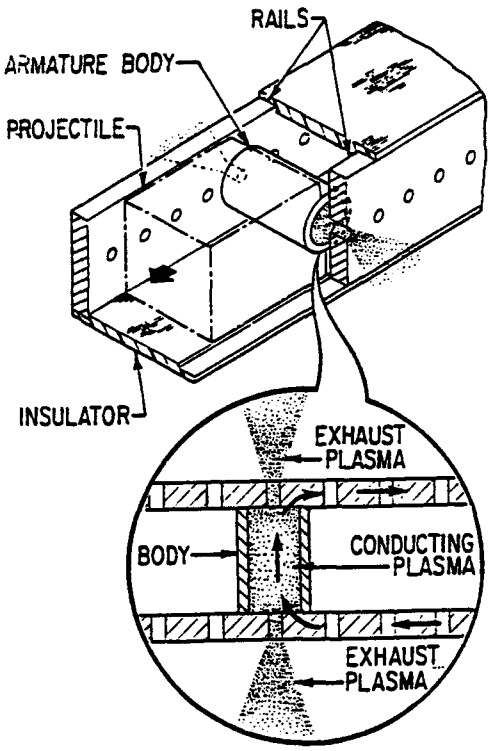

Figure 3. We focussed on venting the plasma out through the rails.

1.2 PHASE I RESULTS.

In Phase I, we did not originally propose venting the plasma out through the rails. We originally pursued a concept that involved a confined plasma armature with the excess plasma being forced out a nozzle behind the armature. The excess plasma would be cooled as it exited the nozzle.[6] As it cooled, the conductivity of the plasma would decrease, thereby reducing the formation of secondary current paths. The concept is shown in Figure 4. There are two difficulties with the original concept. The first is that attaching the nozzle to the plasma confinement chamber is very difficult. The second is more fundamental. The expanding gas is cooled as it leaves the nozzle; however, while the conductivity of the plasma is certainly reduced, it is still substantial. Even if the conductivity of the plasma is reduced by a factor of ten, the gas is still ionized. Normal plasma armatures extend behind the armature for a length of ten or more bore widths. The increase in the conductive area between the rails behind the armature causes the conductance behind the armature to be on the same order (the same or more than) as the armature conductance. Secondary conduction is likely under these conditions. We wanted to eliminate secondary currents as much as possible, so we decided to abandon the original approach in favor of the confined, vented armature with the goal of eliminating residual plasma.

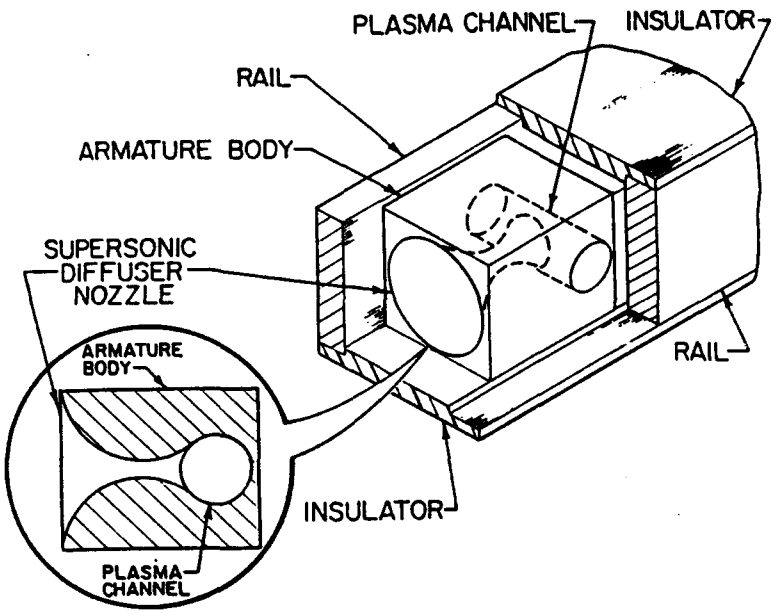

Figure 4. Our original concept used expansion cooling of the plasma to reduce secondaries.

In Phase I, we concentrated on developing structures to contain the high pressures of the confined armature. We used laminated steel containments to prove the feasibility of the concept, then tried Kevlar fiber wrapped containment chambers to reduce the containment mass. Minimization of the containment mass is necessary to maximize velocity performance of the projectile. We obtained encouraging results with this type of containment. The wound Kevlar fiber containment has a higher strength to weight ratio than a containment made of laminated steel. An example (photograph) of the wound containment is shown in Figure 5.

Our work on containment design and testing convinced us that venting is essential. High ohmic power is dissipated in the plasma. This dissipated energy is deposited inside the containment vessel and results (in the nonvented containment vessel) as high pressure and temperature. Theoretically, this high pressure plasma can be contained, but not practicably, as a lightweight launchable projectile.

We concentrated on vents through the rails as the mechanism for pressure control in the armature. The Kevlar containment combined with the rail vents worked well in static tests. However, in actual railgun tests, we had problems with the seal between the edge of the containment and the rail surface. The plasma was contained for a short time, then would leak out between the containment edge and the rail. This quickly caused secondaries to form behind the main armature. A summary of the Phase I railgun tests is shown in Table 1.

We concluded from our work that three things needed to be improved to make the concept work correctly. First, the confined plasma concept should be tested by injecting the projectile into the bore

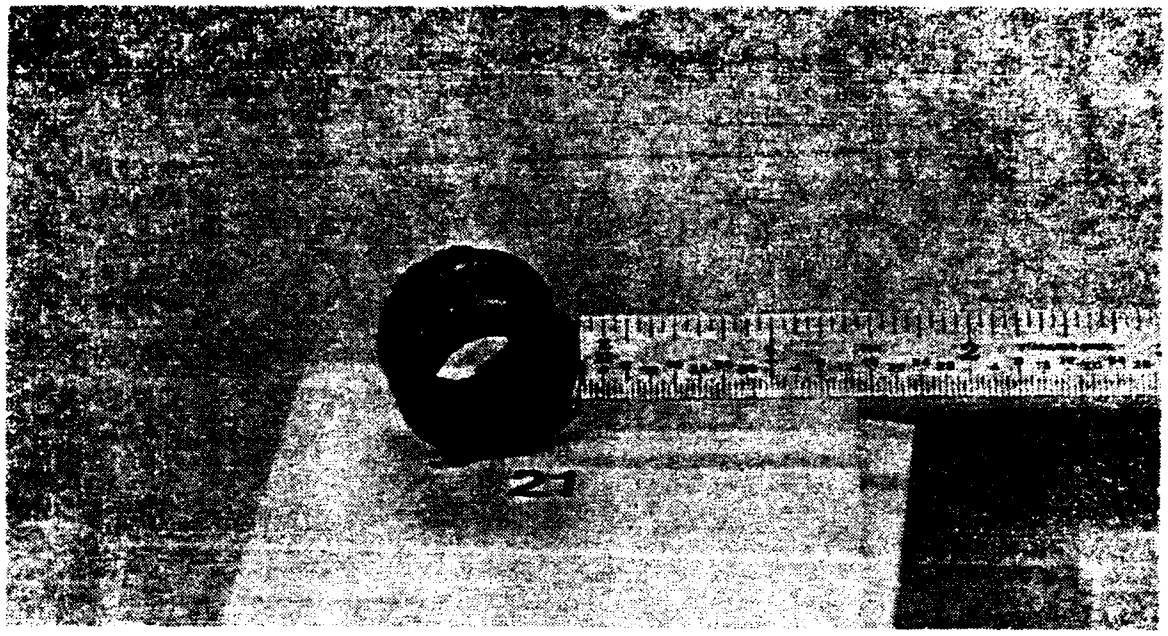

Figure 5. We used wound Kevlar structures to contain the plasma in Phase I efforts.

at a velocity. All of the tests in Phase I were conducted from a static start. This caused excessive erosion of the rail surface around the starting position and was a main contributor to early seal failure.

Injecting the projectile alleviates this part of the problem. Second, we needed to develop a good dynamic seal for the concept. Lastly, we needed to optimize the fiber wound structure and integrate it with the seal design to minimize the projectile mass and maximize the projectile strength.[1]

Table 1. Summary of Phase I Railgun Tests.

Test No.	Armature Shape	Current kA	Final Velocity m/s	Comments
21	Circular	280	500	Partial seal
22	Circular	270	250	Good seal on one rail
23	Circular	280	550	Partial seals on both rails in flight photograph

SECTION 2
PHASE II

2.1 APPROACH.

In Phase II, we concentrated on the two areas we felt would best help us achieve our goals of reaching 6 km/s and eliminating secondary conduction. These are illustrated in Figure 6. One area we focussed on was the seal design. A properly functioning dynamic seal is critical to the success of the concept. Efflux plasma from the containment chamber must be vented out of the bore. Our Phase I tests showed that a simple tight fit between the containment edge and the rail was not sufficient to prevent leakage and secondary currents. We needed to develop an effective, light weight dynamic seal to prevent plasma leakage into the bore behind the projectile for the concept to work properly.

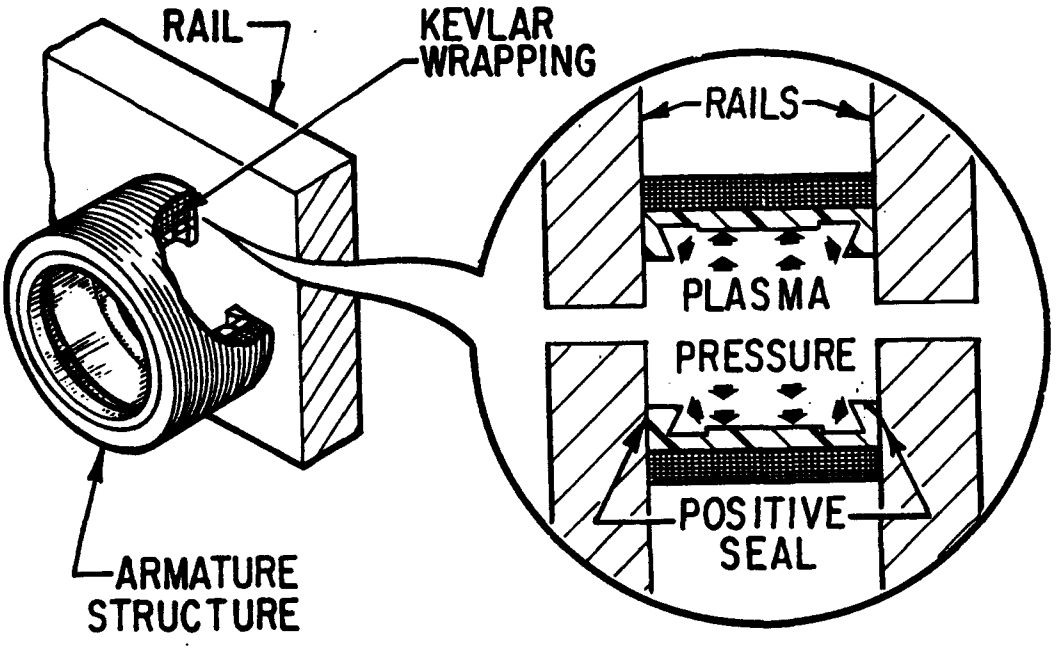

Figure 6. We focussed on pressure control and seal development in Phase II.

The other area we concentrated on was the control of pressure inside the containment chamber. The pressure inside the chamber must be limited so that the chamber does not explode. On the other hand, the chamber pressure needs to be kept high enough for a plasma armature to function properly. If the pressure is too low, the resistance inside the chamber will become too high to support an armature. The result will be that any amount of leakage behind the armature will cause secondary current formation, and will limit the projectile velocity.

We used a focussed approach to study these two areas. The first thing we wanted to do was to perform static tests. These static tests allowed us to determine the relationship between pressure, conductivity, and current density. This was necessary for detailed design of the projectile and barrel. We also used the static tests to develop an effective seal concept.

We then used the knowledge we gained in the static tests to design and fabricate a projectile and barrel for concept testing. These two components must be designed together for the concept to work. We then performed several railgun launches to evaluate the effectiveness of the designs in eliminating secondaries from behind the armature. We used the series of railgun tests to refine the design of the barrel and projectile to make them more effective.

2.2 PRELIMINARY ANALYSIS.

Our first step was to review the requirements for the containment chamber and seals. In general, the conductivity of a plasma increases as the pressure increases, as shown in Figure 7.[7] This indicates that we should try to maintain as high a pressure as possible in the confinement chamber. However, the operational region (pressure and temperature) of the confined plasma is near the "knee" of the curve. In this region, the conductivity is not particularly sensitive to plasma pressure. A factor of ten change in the pressure only results in a factor of two change in conductivity. If we try to maintain a high pressure plasma in the armature, we will not make the conductivity significantly higher than if we maintained moderate pressure levels. Armature voltage and efficiency are not adversely affected by the lower operational pressure. For this reason, we initially believed that heavy, high strength containments would not be necessary.

We determined that we needed to know what the plasma conductivity and pressure do as functions of current density. We also needed to know what the optimum geometry for the confinement chamber and the rail vents were. The static tests provided this data by empirical means, and provided information necessary for scaling the projectile and barrel designs up to levels sufficient to achieve the project performance goals.

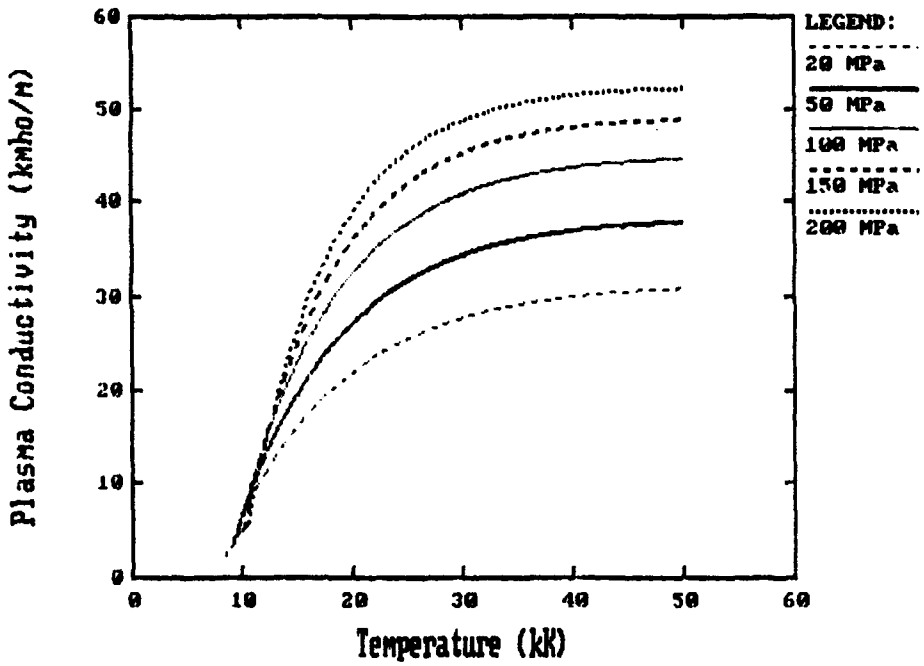

Figure 7. Plasma conductivity is a function of pressure and temperature.

SECTION 3
STATIC TESTS

We performed a series of static tests to provide us with empirical data on the behavior of the plasma conductivity and pressure. Static tests provided a means of gathering this information in a more controlled environment than is possible in a railgun test. The static tests eliminated the effects of velocity and friction, and allowed us to measure the parameters more easily than is possible in railgun tests. This information was essential for the subsequent projectile and barrel design. We needed information on pressure, conductivity, and what affects these two important parameters. In addition, we needed information on the chamber and vent size and geometry as well as scaling data to be able to predict behavior in actual launch conditions. We describe the details of the static tests in the following sections.

3.1 CONCEPT AND DESCRIPTION OF TEST RIG.

We needed a test rig that allowed us to make measurements in an environment that closely simulated the conditions present in a railgun launched confined. We needed a robust test fixture, with few (if any) moving parts. Since the conditions inside the chamber are hostile (high temperature and high pressure), we needed parts subjected to the contained plasma to be either resistant to such an environment, or easily replaceable. Lastly, we needed a low cost, easy to assemble test fixture.

Figure 8 shows a cross section of the test rig. During a test, current flows (positive to negative) from the lower busbar, through the jumper, and into the unvented electrode. A plasma is created in the containment chamber by exploding the fuse that connects the unvented electrode to the vented electrode. Current then flows through the vented electrode, through the aluminum pressure containment, into the upper busbar, and returns to the power supply. The assembled test rig is shown in a photograph in Figure 9.

The interior of the containment chamber is insulated from the outer aluminum containment by a G-10 tube. Plasma leakage is prevented by O-rings on the sides of the unvented electrode (grooves were cut into the electrode) and O-rings between the vented electrode and the aluminum containment (grooves for these O-rings were cut into the top face of the aluminum containment). The busbars are clamped to prevent excessive deflection, and the vented electrode is clamped to the top of the containment. The clamps are electrically isolated from the current carrying parts of the structure. The unvented electrode is free to move vertically, so that we could measure the pressure inside the chamber. The unvented electrode rests on a force transducer which measures the force that the expanding plasma exerts on the electrode. We discuss instrumentation in the next section.

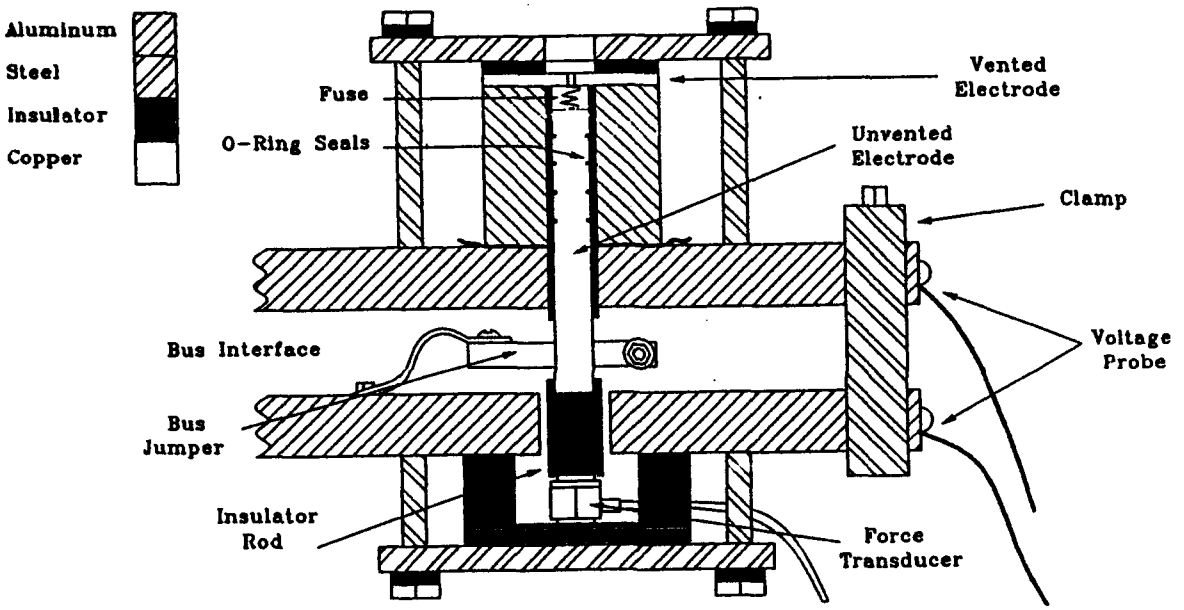

Figure 8. The static test rig is a simple device.

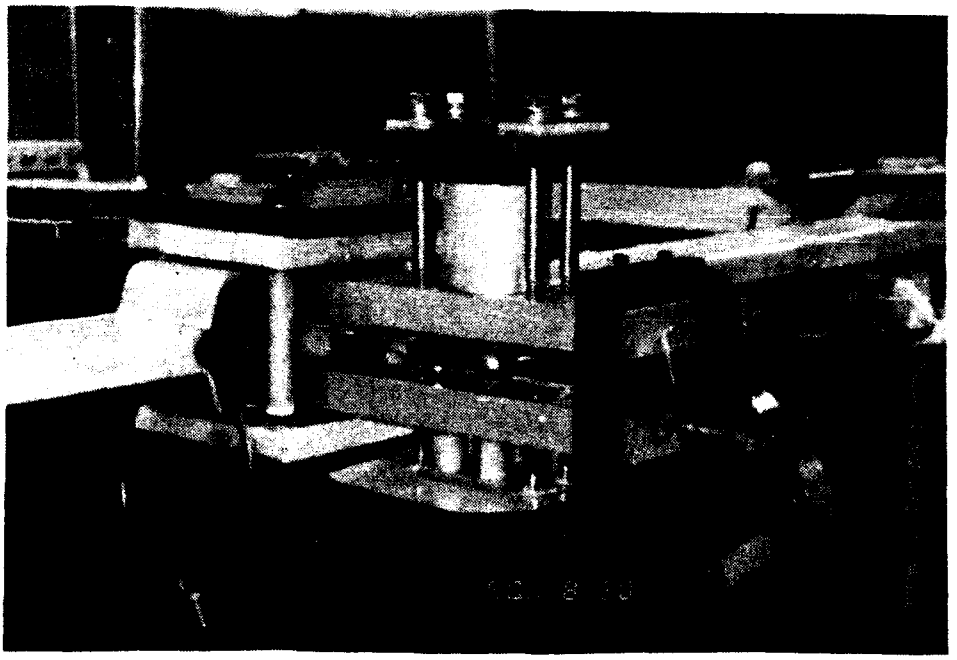

Figure 9. We used the above static test rig to measure confined plasma properties.

3.2 INSTRUMENTATION.

We measured three quantities for each test. We measured the current flowing through the chamber, the voltage between the vented and unvented electrodes, and the force exerted on the unvented electrode by the expanding plasma. We measured the current with a calibrated Rogowski coil. This coil is part of the standard diagnostics for the power supply, a 210 kJ capacitor bank capable of currents up to 360 kA, but maximum current for these tests was 130 kA. A typical current waveform is shown in Figure 10.

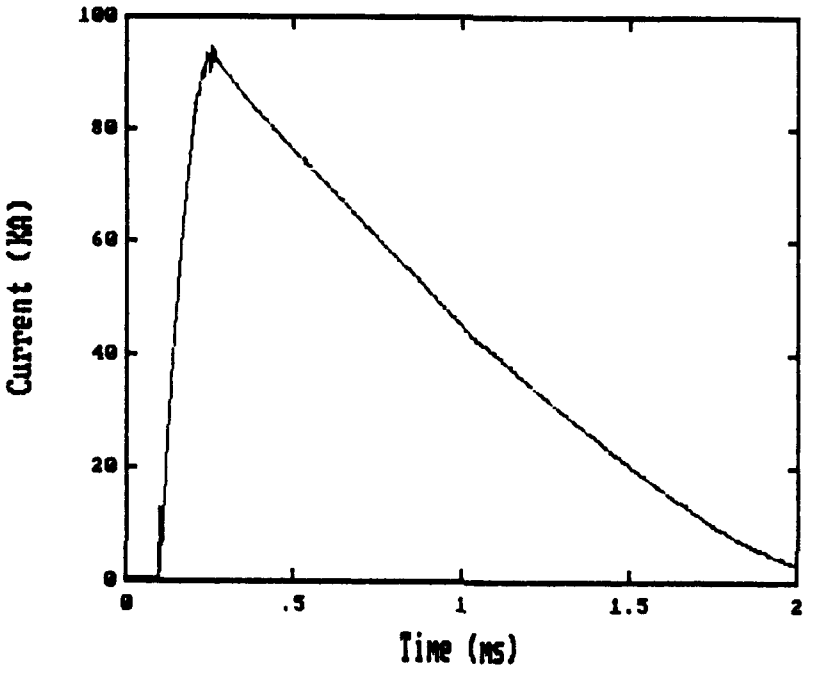

Figure 10. The current pulse typically lasted about a millisecond.

We measured the voltage with a shunt resistor connected between the upper and lower busbars. The value of this shunt resistor (on the order of 10 Ω) is very large compared to the resistance of the experiment (on the order of mΩ). We determine the voltage by measuring the current through the shunt resistor with a current transformer. The current transformer provides electrical isolation between the experiment and our data recorders. The maximum voltage for these tests was 500 V. A typical voltage waveform is shown in Figure 11.

The pressure measurement presented us with some difficulty. Initially, we tried to measure pressure using a capillary tube inserted into the containment chamber and connected to the input of a pressure transducer which responds directly to pressure. We abandoned this approach after several attempts because we did not obtain believable measurements. The capillary tube melted during each test, making the results dubious.

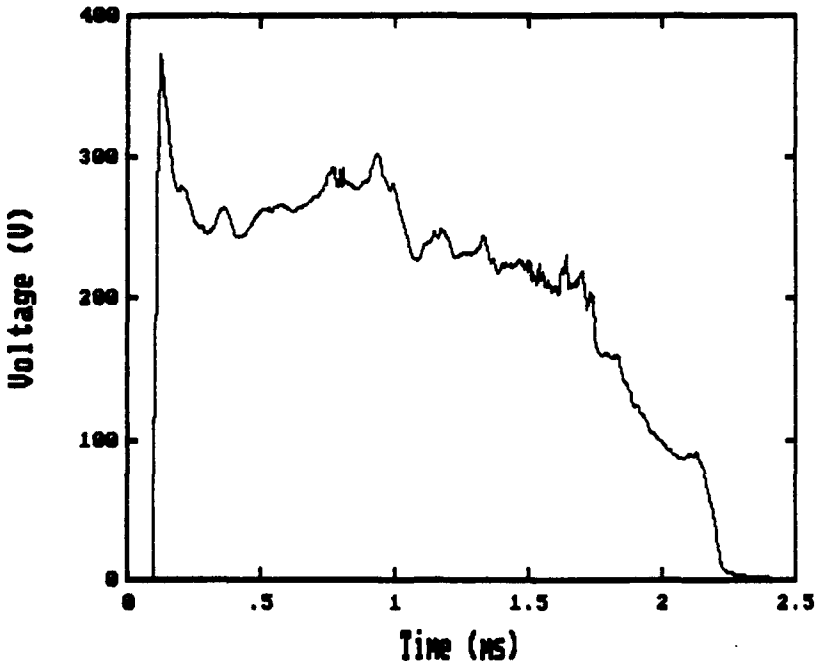

Figure 11. We measured the plasma voltage.

We then decided to measure the force on the unvented electrode, and derive the pressure from that measurement. As we described in the previous section, the vented electrode is free to move vertically, as shown in Figure 8. The unvented electrode rests on an insulating block, which rests on the force transducer (piezo-electric crystal). Thus, we take the force exerted on the rod by the expanding plasma, and divide it by the cross sectional area of the electrode to obtain the plasma pressure. We assume that the plasma pressure is uniform across the face of the unvented electrode. The force required to overcome the friction from the O-rings is negligible compared to the force exerted by the expanding plasma.

A typical pressure waveform is shown in Figure 12. The pressure should follow the current waveshape. The mechanical response of the electrode, insulator, and transducer produce the vibrations seen in the figure. We believe that the measurement is accurate up to the peak value. We were mostly concerned with the peak pressure value as a worst case design condition. The maximum pressure we saw during these tests was 165 MPa. We used the peak value in our analysis.

The position of the bus jumper imposes a magnetic repulsion between the jumper and the upper busbar. This repulsion exerts an additional force downward on the unvented electrode. We measured this repulsion during tests with a solid aluminum short in the containment chamber (no plasma effects). Since the magnetic force is proportional to the square of the current, we can scale the effect for different current levels. We compensate our peak pressure measurement for magnetic repulsion by subtracting the scaled magnetic effect (peak) from the measured value.

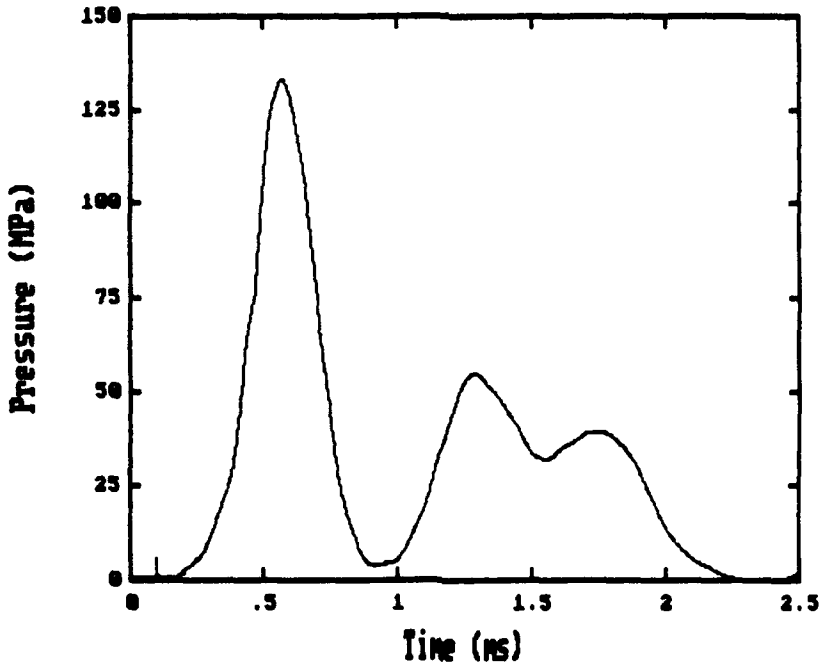

Figure 12. The pressure measurement is accurate up to the peak.

We calculated the current density by dividing the current waveform by the cross sectional area of the unvented electrode. We derived the conductivity from the voltage and current measurements. We used the relationship for a uniform media:

$$R = l/\sigma A \tag{1}$$

where R is the resistance,

σ is the plasma conductivity,

l is the length of the plasma chamber, and

A is the cross sectional area of the chamber.

The conductivity is then given by:

$$\sigma = l/RA \tag{2}$$

The resistance, R, is simply the measured voltage divided by the measured current. This is shown in Figure 13. A sample of the derived conductivity is shown in Figure 14.

We summarize our static test results in the next section.

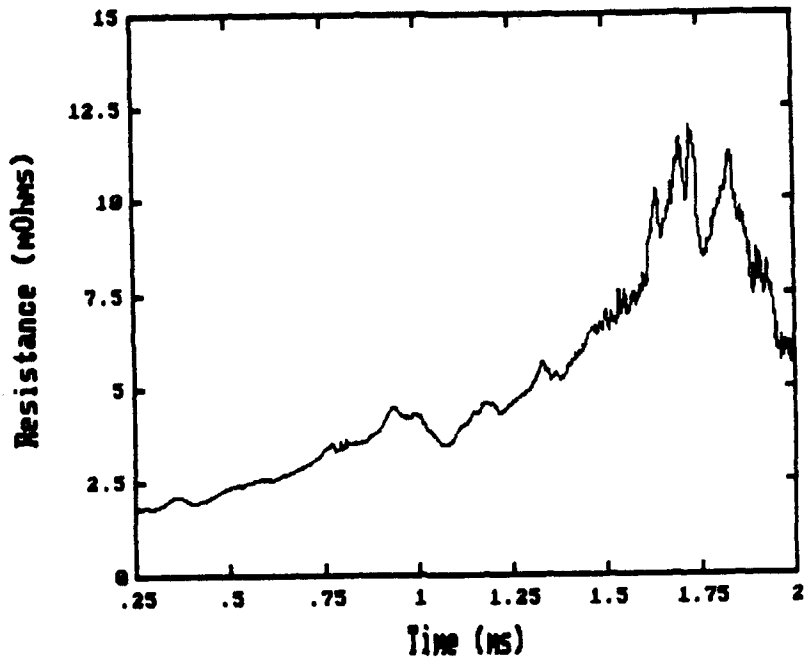

Figure 13. We calculated the plasma resistance from our measurements.

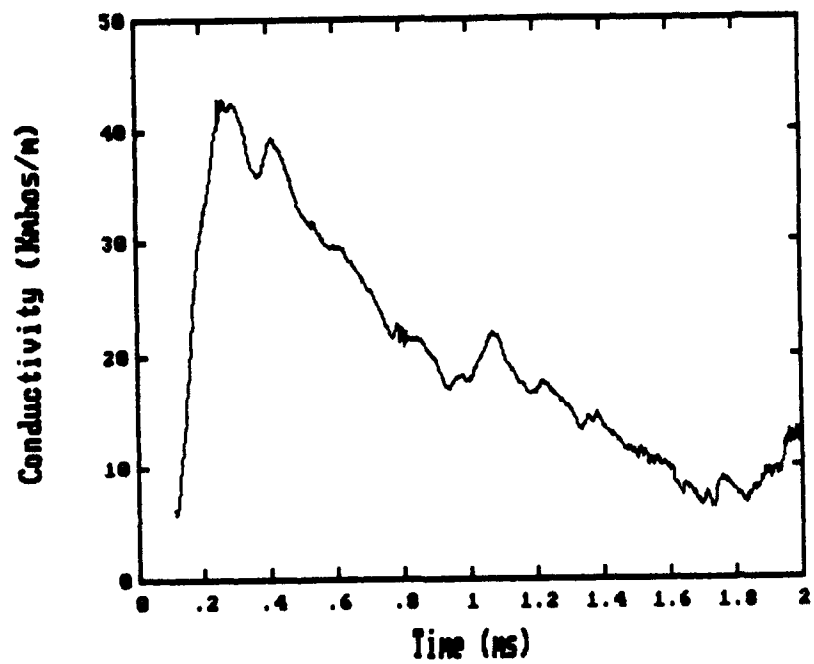

Figure 14. We derived the plasma conductivity from the resistance and the geometry.

3.3 RESULTS.

We performed a total of 35 tests with the static test fixture. Ten tests were seal tests. We will discuss the results of the seal tests in the next section. Of the remainder, fifteen used the force transducer to obtain the plasma pressure. The results are summarized in Table 2. We tested vent diameters from 3.18 mm to 9.5 mm (11.1 mm in the seal tests).

Table 2. Summary of Static Tests.

Test No.	Transducer Type	Current (kA)	Vent Hole Size (mm)	Peak Conductivity (kmhos/m)	Mean Conductivity (kmhos/m)	Peak Pressure (MPa)	Mean Pressure (MPa)	Comments
1	Pressure	105						Shorting Test-No Plasma-Arcing
2	Pressure	95						Shorting Test-No Plasma-Arcing
3	Pressure	110						Shorting Test-Nc Plasma-Arcing
4	Pressure	110						Shorting Test-No plasma-No Arcing
5	Pressure	110						Shorting Test-No plasma-No Arcing
6	Pressure	95	6.30	36.16	20.40	---		Bad Pressure signal
7	Pressure	97	6.30	40.53	20.50	---		Strange Pressure Signal
8	Pressure	92	6.30	28.24	15.70	---		Strange Pressure Signal
9	Pressure	94	6.30	31.24	17.00	---		Strange Pressure Signal
10	Pressure	95	3.18	40.76	25.40	---		Strange Pressure Signal-dI/dt
11	Force	92	4.70	41.54	20.17	24.47	28.2	New Force x-ducer/Clamp around bus bars/ringing
12	Force	93	4.70	32.00	17.70	97 (est)	---	Clamped to each bus bar/no ringing
13	Force	98	4.70	40.70	23.40	---		Lost Force Signal Due to Atten.
14	Force	95	4.70	42.77	18.2	101.63	47.7	
15	Force	98	6.35	(35) (???)	---	33.75	28.6	No Voltage Signal
16	Force	60						Shorting Test-signals attenuated too much
17	Force	59						Shorting Test-Neg. Force sig. looks like V
18	Force	120						Shorting Test-Neg. Force sig. looks like V
19	Force	130						Shorting Test-Neg. Force sig. looks like V
20	Force	98						Shorting Test-Flexible braid blew
21	Force	100						Shorting Test-Short actioned-good force signal
22	Force	96						Shorting test-bad voltage signal
23	Force	90	6.35			72.97	48.9	Bad voltage signal
24	Force	90	6.35	34.52	16.10	36.23	38.1	
25	Force	90	9.50	28.99	14.50	31.68	25	

We found that the plasma pressure was related to the experimental parameters of vent size, current density, and power density. We used a graphic presentation of the data in the table to show the trends of the data more clearly. The plasma pressure decreases as the vent diameter increases, as shown in Figure 15. The peak plasma pressure increases with the current density, as shown in Figure 16. The plasma pressure also increases with the power density in the plasma, as shown in Figure 17.

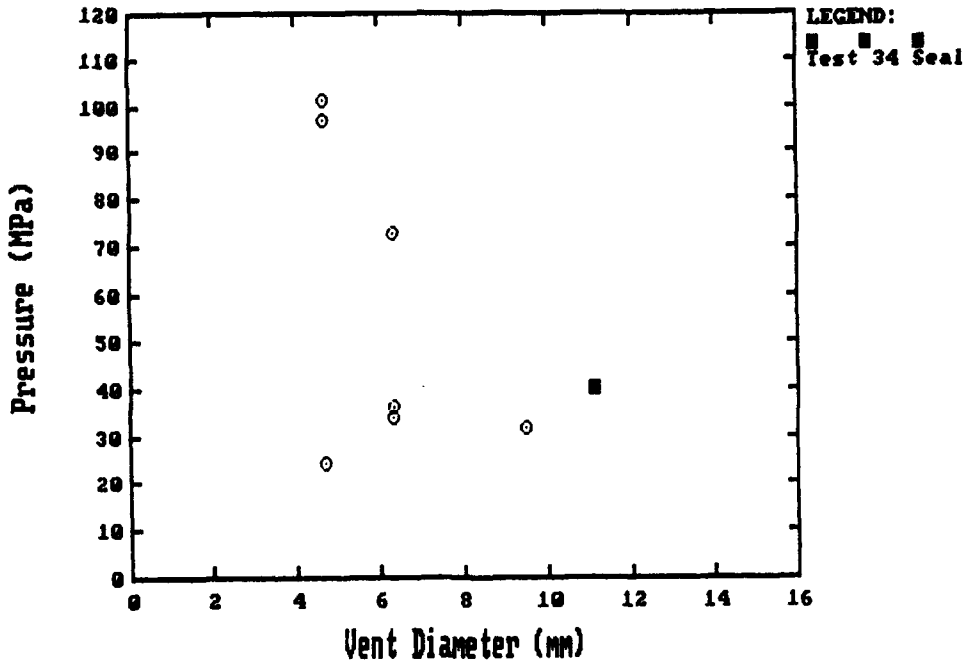

Figure 15. The plasma pressure decreases as the vent diameter increases.

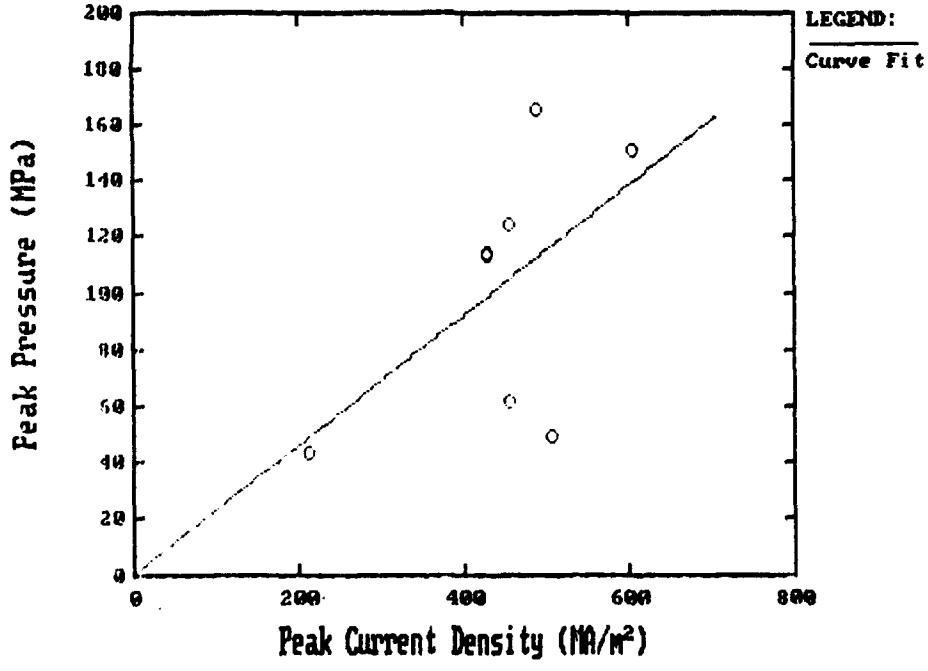

Figure 16. The plasma pressure increases with the current density.

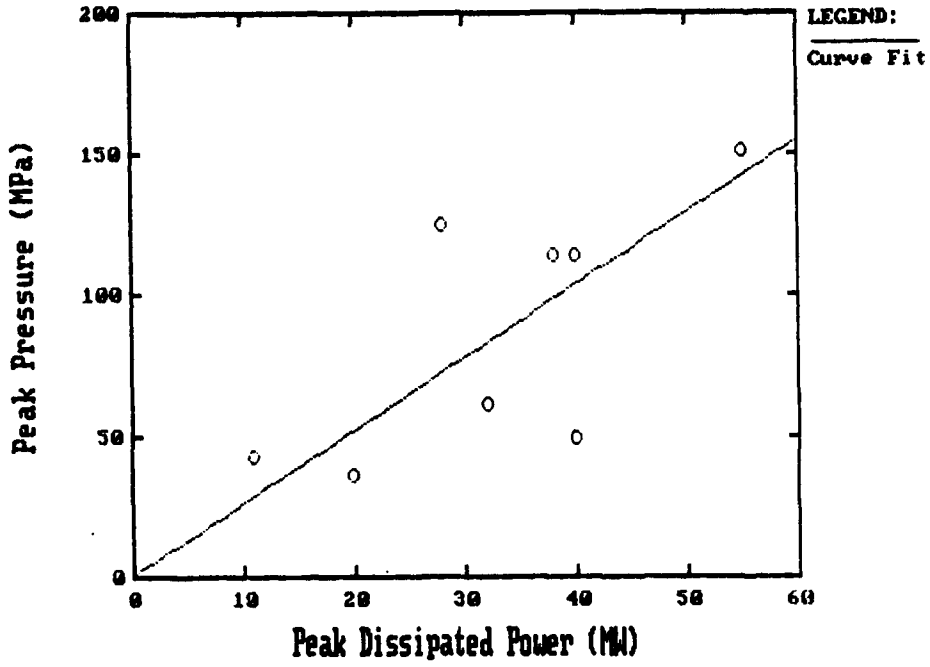

Figure 17. The plasma pressure increases with the power density.

The conductivity of the plasma was only a weak function of vent size (pressure), as shown in Figure 18. Our data confirmed our preliminary analysis.

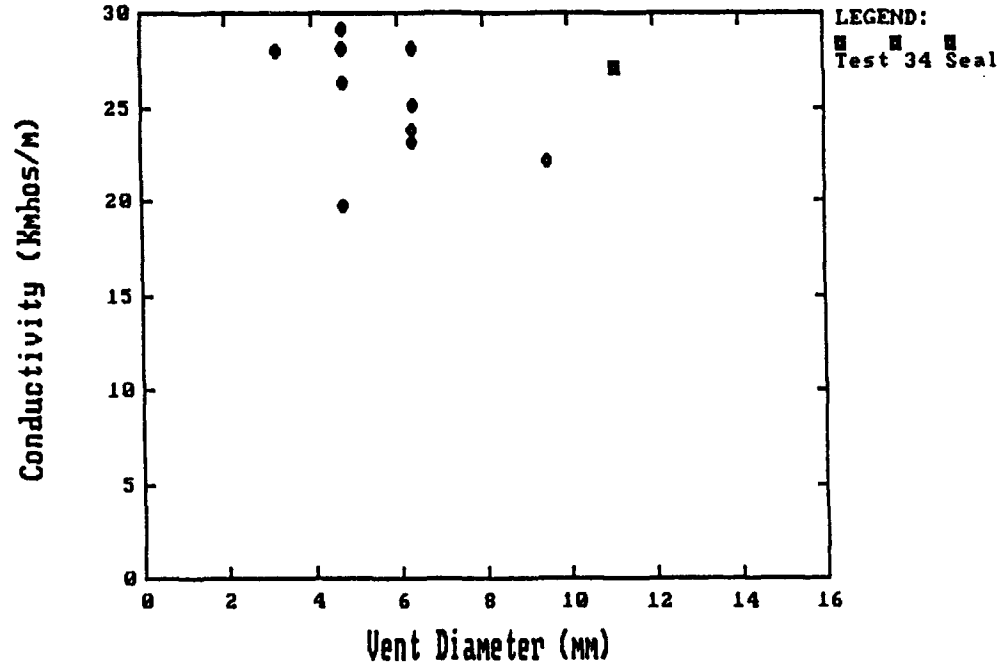

Figure 18. The conductivity is only a weak function of pressure.

From these tests, we obtained data upon which we could base subsequent projectile and barrel designs. We had to normalize the vent size to be able to scale parameters to realistic railgun levels. We divided the vent area by the cross-sectional area of the containment chamber to normalize the vent size.

The pressure data for normalized vent sizes appears in Figure 19. The ratio of vent area to chamber area can vary from 0 to 2.0 (there are two chamber ends), even though only 0 to 1.0 is shown.

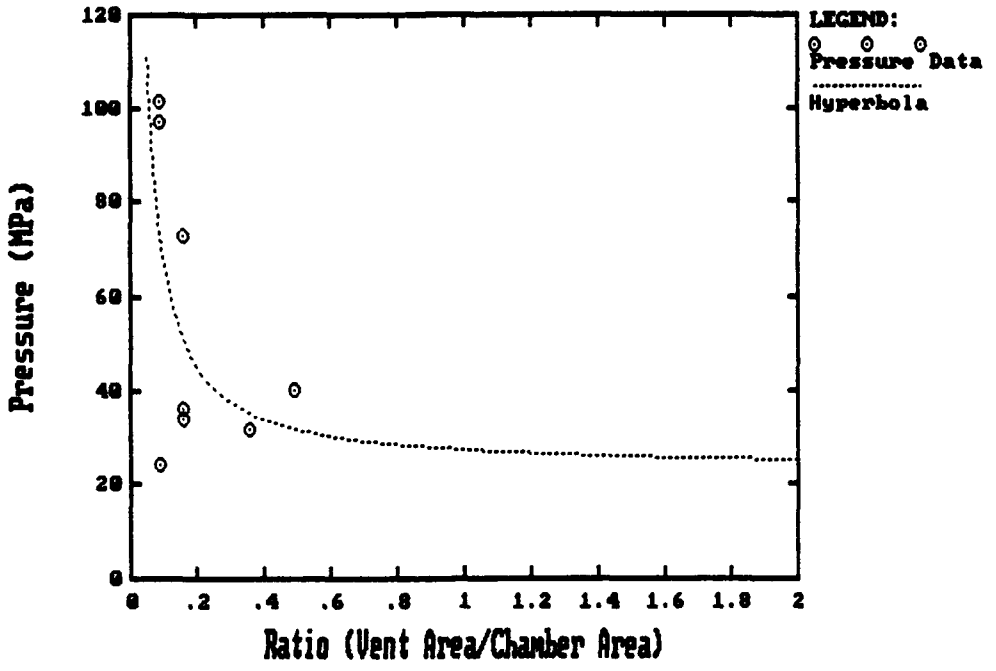

Figure 19. The pressure decreased as a function of the normalized vent area.

We assumed a linear relation between the pressure and the power density. Since the voltage stays relatively constant as the current density increases, we decided that the power density and the current density showed essentially the same information (a linear relation). Current density was on the order of 0.5 GA/m^2 for these tests, but we could easily scale up to launch conditions (possibly as high as 8-10 GA/m^2). This extrapolation is shown in Figure 20, using the linear curve fit shown in Figure 17.

Since the conductivity is not a strong function of the pressure in the operational region in which we were interested, we can reduce the pressure requirements to optimize the launch package mass. If we reduce the pressure from the order of GPa to hundreds of MPa, we can substantially reduce the mass required to contain the plasma pressure and to seal the bore without sacrificing energy efficiency of the launch package.

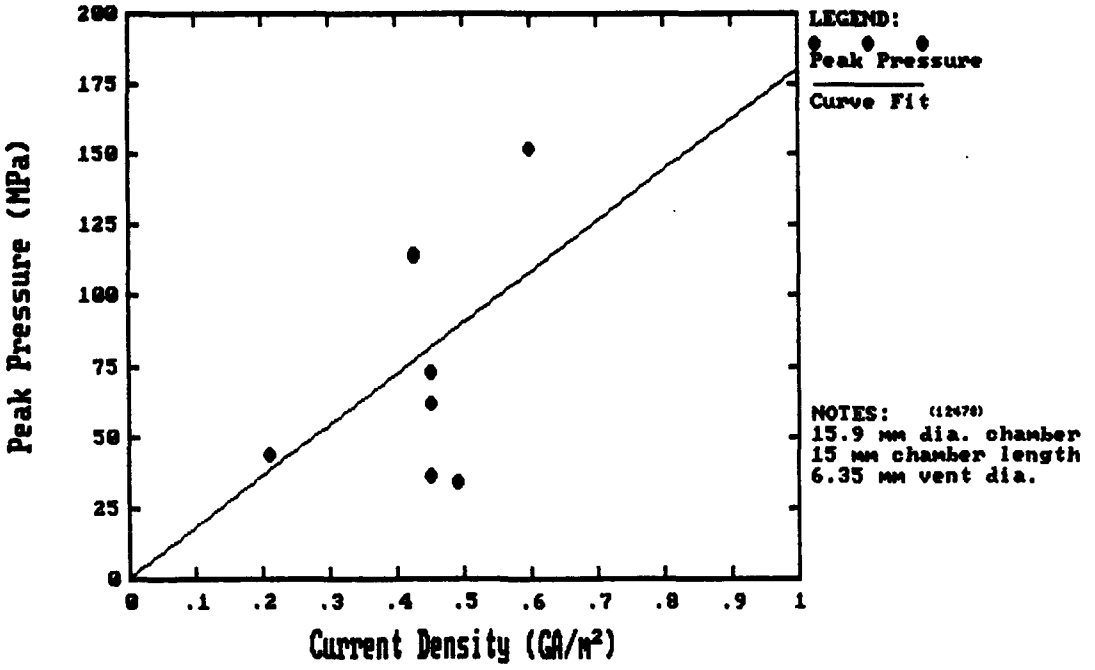

Figure 20. We extrapolated pressure as a function of current density for launch conditions.

We used the static test fixture to learn more about sealing at the containment-rail interface. We will discuss the static seal tests in the next section.

3.4 SEAL TESTING.

The method we use to seal the bore from the venting plasma is critical to the success of this armature concept. If the seal allows sufficient plasma behind the armature, secondary current conduction will occur and we will not achieve our performance goal. We used the static test fixture to evaluate a seal design concept. In this section we will discuss the seal concept, the changes we made to the test fixture, and the results we obtained.

3.4.1 Labyrinth Seals.

We originally considered a lip seal on the plasma containment chamber as depicted in Figure 6 to eliminate leakage. In this concept, the seal is positively actuated by plasma pressure. The problem with this concept is that the lip of the containment provides limited surface area for proper seal function. The lip tends to be broken/sheared off as if moves across a rail vent hole.

We decided to concentrate on labyrinth seals for restricting plasma leakage. The concept is shown in Figure 21. This concept provides a bore seal both in front and behind the armature. By placing the seal on a sabot rather than on the chamber lip, we can use much more surface area to seal the plasma.

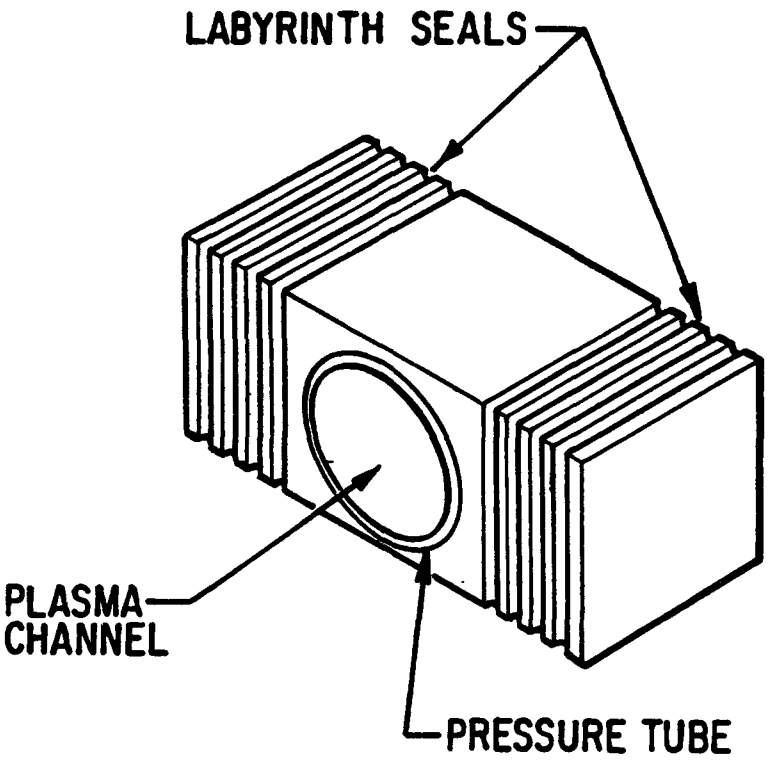

Figure 21. We used labyrinth seals to prevent secondary currents.

A labyrinth seal is basically a series of grooves and blades between the high pressure and low pressure regions. In this type of seal, the leaking gas flows along the bore wall, over a blade and into the next groove. The blades provide restrictions to the flow. At each change in the cross sectional area of the flow, a pressure drop occurs. Thus, the more blades in the seal, the less leakage will occur, and the greater the pressure reduction. The plasma that leaks through the seals is radiately cooled by the walls of the bore and the seal. In addition, a small amount of expansion cooling occurs in the seal itself. This cooling will reduce the temperature of the leaking plasma and reduce the probability of secondary current in front of and behind the armature.

Literature is available for the design of labyrinth seals, but design relations lack much detail, and are very design dependent.[8] We performed static seal tests to establish guide lines to be able to use labyrinth seals effectively in the projectile design.

Performance of seal tests on the static test fixture required some modifications to the fixture. We will discuss these modifications in the next section.

3.4.2 Alterations to Test Apparatus.

We had to modify the test fixture to perform seal tests. First, we had to change the unvented electrode to fit a seal into the chamber. We used a 0.25" diameter copper rod for the electrode and fit

the seal around the rod. A typical test seal is shown in Figure 22. Some of the seals we tested were made of Lexan (polycarbonate). Others were made of Nylatron GSM (an extruded nylon derivative with molybdenum disulfide particles suspended in it for added strength). We chose these materials as the best probable candidates for use in the later railgun launches. Both are lightweight electrical insulators. We favored the use of Nylatron for its superior strength. Nylatron is also slightly less dense than Lexan.

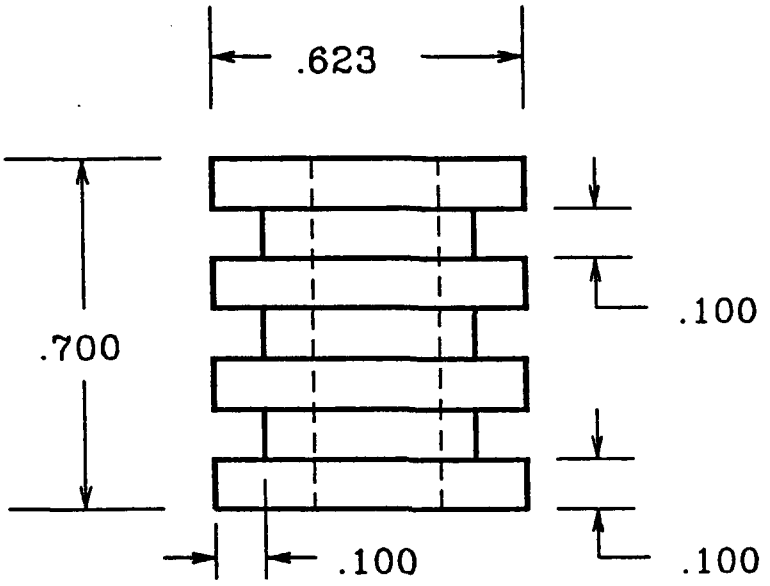

Figure 22. Our test seals were typically Lexan or Nylatron.

The cross section of the top part of the test fixture is shown in Figure 23. This view shows the seal and the addition of a breakdown detector to the test fixture. The breakdown detector is simply two wires at a known separation with a voltage imposed between them. We put approximately 500 V between the wires. If the gap between the wires breaks down, current will flow in the circuit created by the wires, the gap, and the power supply. We limit the current in the circuit with a resistor, and measure the current through the resistor with a current transformer. If the gap does not breakdown, there will be no (0 V) signal. If sufficient plasma leaks past the seal under test, we will detect it in our probe. Figure 24 shows a typical signal in which an electrical breakdown occurred between the wires of the probe.

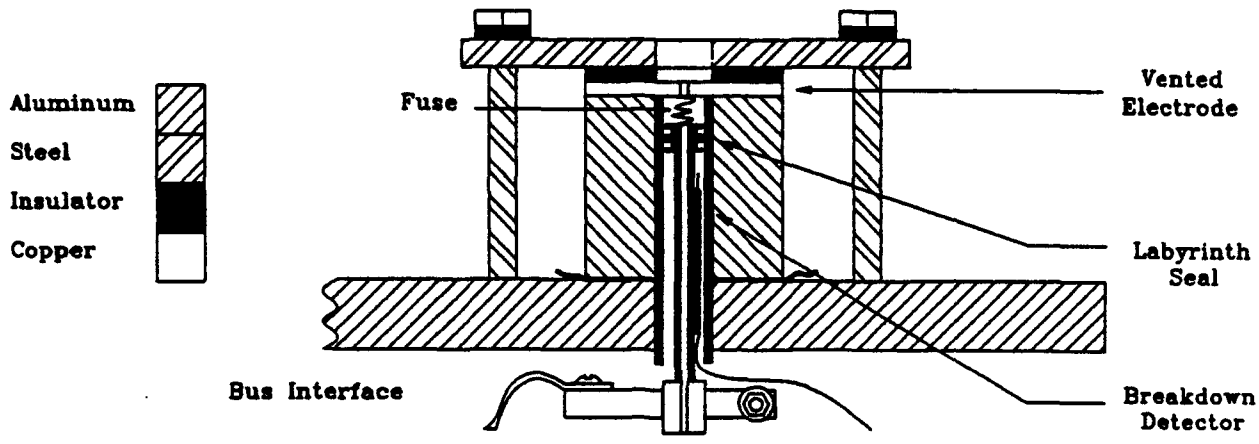

Figure 23. We modified the test fixture to incorporate seals and a breakdown detector.

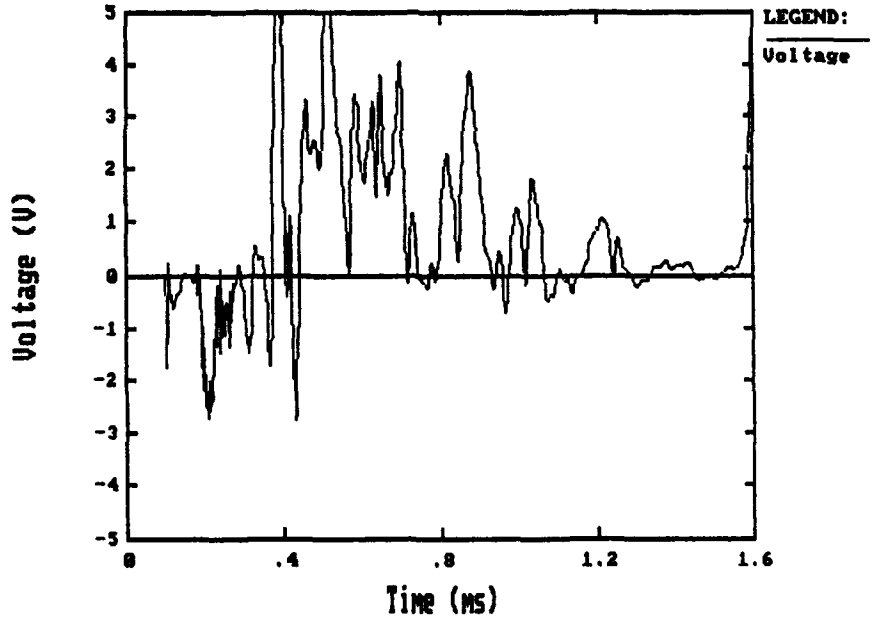

Figure 24. Our breakdown detector worked well.

The peak electric field between the wires is set by the spacing of the wires and the imposed voltage. We chose these values to create an electric field under the seal that would approximate the field present in the bore behind the armature. If sufficient plasma leaked past the seal to cause a breakdown in the probe, we knew that the leak rate was too high for the seal design to be useful in a railgun test. We could then establish a maximum leak rate for the effective operation of the seal with our confined plasma armature. We will discuss the results of our seal tests in the next section.

3.4.3 Results.

We performed a total of ten seal tests. The results are summarized in Table 3. We tested seals with a range of clearances. We also varied the number of blades in the seal. The table shows that only one seal showed no breakdown behind the seal. This was a four-bladed seal with 0.001" radial clearance with a 11.1 mm vent diameter. We computed the leak rate in this test to be 0.03 kg/s. Seals with a larger clearance all exhibited significant breakdown. We took this leak rate to be a maximum for our projectile design. We will discuss seal design and leak rate more in the next section. In a test with a four bladed seal at higher pressure (6.35 mm vent diameter), two of the seal blades broke, demonstrating the need for strong blades.

Table 3. Summary of Seal Tests.

Test No.	Date	Transducer Type	Current (kA)	Vent Hole Size (mm)	Plasma ch. Length (mm)	Peak Conductivity (kmhos/m)	Mean Conductivity (kmhos/m)	Peak Pressure (MPa)	Mean Pressure (MPa)	Breakdown under seal?	Radial Spacing (mm)	Number of blades on seal
26	09/19/90	Force	100	6.35	15	18.43	7	49.28	25.4	Y	.127	1
27	09/20/90	Force	90	6.35	15	27.3	15.2	124(est)	---	Y	.127	2
28	09/20/90	Force	42	6.35	15	16.21	10.3	43.13	12.5	Y	.127	3
29	09/21/90	Force	97	6.35	15	26.04	15.6	165.45	66.2	Y	.127	4
30	09/28/90	Force	100	6.35	15	?	?	?	?	?	.064	1
31	10/01/90	Force	90	6.35	15	21.82	8.8	61.90	57.14	Y	.064	2
32	10/01/90	Force	85	6.35	15	19.00	10.8	113.71	79.09	Y*	.064	3
33	10/01/90	Force	85	6.35	15	15.70	8.1	113.30	72.76	Y	.064	4
34	10/04/90	Force	95	11.11	15	27.12	8.5	40.04	30.52	N	.025	4
35	10/05/90	Force	120	6.35	15	31.25	9.8	151.39	76.72	Y*	.025	4

* Slight Breakdown in seal

The table emphasizes the important results of the seal tests. The first result is that the seal clearance must be minimized. This must be done to minimize the leakage past the seal. The second result is that the seal blades must be robust. We must design the seal blades to withstand the shear loads introduced by the high pressure drop that will be present in railgun launches.

The last important result from the seal tests is that the leak rate must be kept low. This is necessary to prevent secondary current conduction behind the armature, and is essential to the success of the confined, vented armature concept. We used the information we obtained from all the static tests in our projectile and barrel design. We will describe the design process for the railgun launches in Section 4.

SECTION 4

DESIGN AND FABRICATION OF THE PROJECTILE AND BARREL

The launcher system consists of four components: the power supply, the railgun barrel, the injector, and the projectile. Of these components, the power supply and the injector are fixed (except for minor modifications). The power supply sets the upper limit on the energy available for the launch. The injector sets the maximum initial projectile velocity. We will discuss how these components impact the design of the projectile and barrel in this section. We will also describe the details of the design process for the projectile and barrel.

4.1 PROJECTILE.

Our power supply is a 1.7 MJ capacitor bank. This power supply can deliver up to 1 MA to a railgun load. The system inductance is 3 μH, and the system resistance is 200 $\mu\Omega$. This limits the amount of energy available to accelerate the projectile. Figure 25 shows how the available power limits the mass we can accelerate. For a 3 m barrel with an inductance gradient of 0.37 μH/m, we can achieve 6 km/s with a mass no greater than 16 g. This sets an upper limit on the mass as well as the size of the projectile. The bore size is limited to 15 mm by 20 mm if we assume a solid polycarbonate projectile 45 mm long.

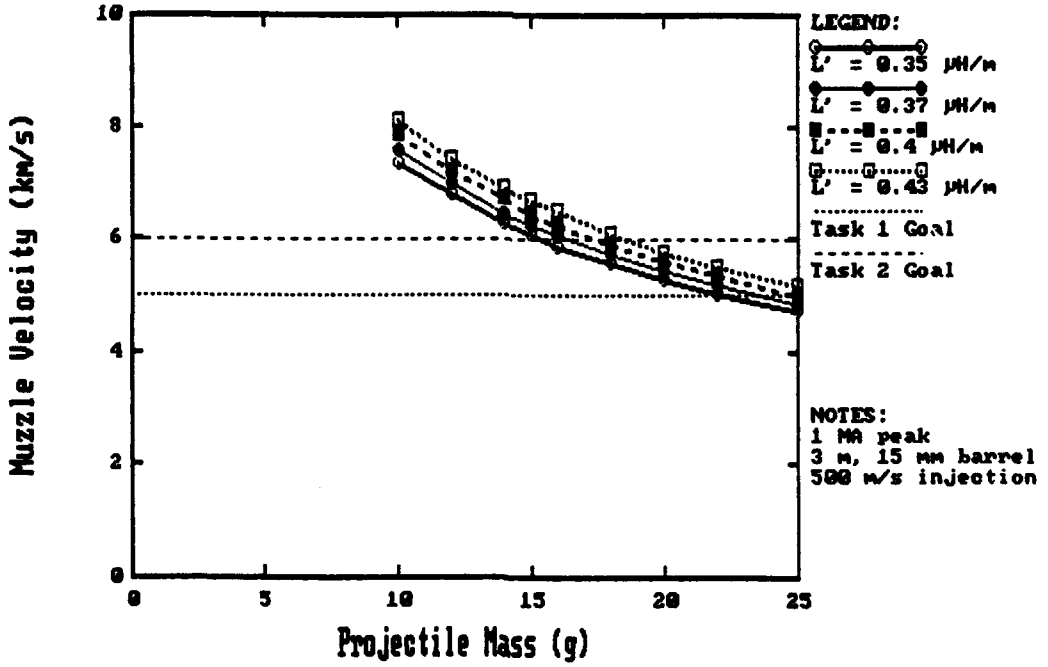

Figure 25. Final velocity is limited by the projectile, launcher, and power source.

We determined that we could achieve 5 km/s with a 14 g projectile and 800 kA peak current. This would be a significant intermediate step toward the 6 km/s barrier. If the armature concept functioned well at the intermediate level, we felt that exceeding 6 km/s would only require optimization and

refinement of the design of the barrel and projectile. This 800 kA peak current also determines that the minimum requirement for the barrel inductance gradient is 0.37 μH/m.

We wanted to design an integrated projectile which incorporated the plasma containment and the front and rear seals. This approach minimizes the projectile mass. The projectile has three constituent parts: the plasma containment vessel, the seals, and a means of keeping the containment and seals together. The 800 kA current establishes a current density inside the containment of about 7.5 GA/m^2. We used the data from the static tests to extrapolate a maximum pressure for the plasma inside the containment. The data is shown in Figure 20. This data is for a current density of 0.5 GA/m^2. The dashed line represents the hyperbola we used to fit the data. With a vent area to chamber cross section ratio of 0.7, we essentially minimize the pressure inside the chamber. Above this ratio, the pressure will not decrease significantly. Below this ratio, the pressure increases dramatically.

We then used the current density/pressure data in Figure 21 to determine the maximum operating pressure. That data and curve fit are for 0.5 GA/m^2 and a vent area to chamber cross section of 0.16. The pressure scaled for the larger vent size at 7.5 GA/m^2 is 400 MPa. This is the operating pressure we based our design on.

Once the peak current and pressure were set, and we knew what the minimum inductance gradient was, we computed the projectile acceleration. The acceleration profile determines the stress on the projectile. We then started the design of the containment vessel.

We first looked at candidate materials to construct the pressure containment. We obviously needed a material that was both lightweight and strong. In Phase I we used a unidirectional Kevlar tape preimpregnated with epoxy. We constructed the Phase I pressure chambers by winding this tape on a form then curing the epoxy at 250°F. The Kevlar tape was exceptionally strong and light. We found a graphite fiber preimpregnated tape which was lighter and stronger than the Kevlar. We used this tape in the construction of both the pressure chamber and the projectile containment.

We approximated the chamber as a thin walled pressure vessel. We estimated the projectile mass to be 14 g. Using the manufacturer's material properties for the graphite tape, we determined that we could construct a cylinder made of the tape to serve as a pressure vessel. The cylinder has a 15 mm outer diameter, 11.5 mm inner diameter, and 15 mm length. To construct the projectile, we placed the seals on either side of the pressure chamber, then wrapped the entire structure with the graphite tape. This overwrap held the projectile together during launch. The graphite overwrap must be 2.5 mm thick to hold the projectile together at 800 kA. This makes the bore dimensions 15 mm rail-to-rail and 20 mm between the insulators.

The seals must be designed to drop the pressure of the leaking plasma to a point where secondary

currents will not occur. A further consideration was that the seal blades must withstand the high pressure exerted on them without breaking.

In order to withstand the containment vessel pressure, we chose a phenolic laminate, G-10 as the labyrinth. The main problem with a laminate such as G-10 is that the material strength depends on the orientation direction of the fibers which comprise the layers. Using G-10 makes the projectile heavier. We drilled out the parts of the G-10 seals that were not absolutely essential to the structure to minimize mass.

The leakage rate from a labyrinth seal, W, is given by the equation:

$$W = 25KA\sqrt{\frac{\left(\frac{P_1}{V_1}\right)-\left[1-\left(\frac{P_2}{P_1}\right)^2\right]}{\left[N-1n\left(\frac{P_2}{P_1}\right)\right]}} \qquad (3)$$

where N is the number of blades,

W is the flow rate in lb/hr,

V_1 is the initial specific volume in ft^3/lb,

K is a coefficient determined by the geometry of the seal,

A *is the leaking area* determined by the clearance in in^2,

P_1 is the inlet pressure in psi, and

P_2 is the outlet pressure.

We used this relation to establish the minimum leak rate of 0.03 kg/s in the static tests. We assumed a P_2/P_1 of 0.1.

We decided to make the front seal shorter than the rear, to reduce the projectile mass. The rear seal is the more critical. If the front seal leaks too much, a precursor arc will form. Precursors containing up to 30% of the total current are not detrimental to the projectile performance. Excessive leakage from the rear seal causes secondary currents and reduces the projectile acceleration.

The design is shown in Figure 26. The rear seal has three blades, and the front only has two. The blades and grooves are the same width (initially 3.34 mm). The groove depth is half of the width (1.67 mm). This seems to be the optimum trade between the seal effectiveness (number of blades) and blade strength. We did the final sizing of the projectile after each barrel was assembled. This ensured that we would at least initially have a seal clearance of 0.001" or less (less would decrease the leak rate). If we assume an initial pressure of 400 MPa, the final pressure would be 200 MPa, and the designed leak rate is 0.03 kg/s for the rear seal, but the front seal leakage is higher, about 0.04 kg/s.

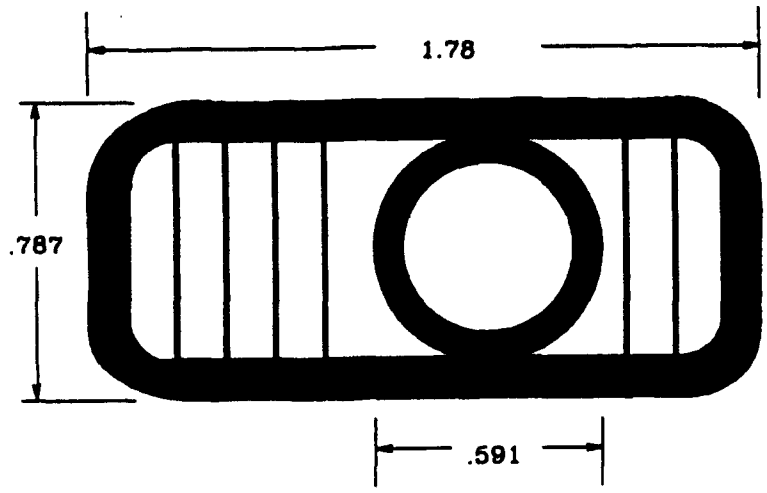

MATERIAL: Inner constuction G-10.
Outer wrapping is a unidirectional
graphite fiber composite, as is
inner plasma containment vessel.

Figure 26. The projectile integrates the seals and pressure vessel.

After we completed the design, we performed a finite element analysis on the projectile structure. This analysis confirmed our stress calculations on the projectile. The structure should perform up to the 800 kA level necessary for 5 km/s. A photograph of the assembled projectile is shown in Figure 27.

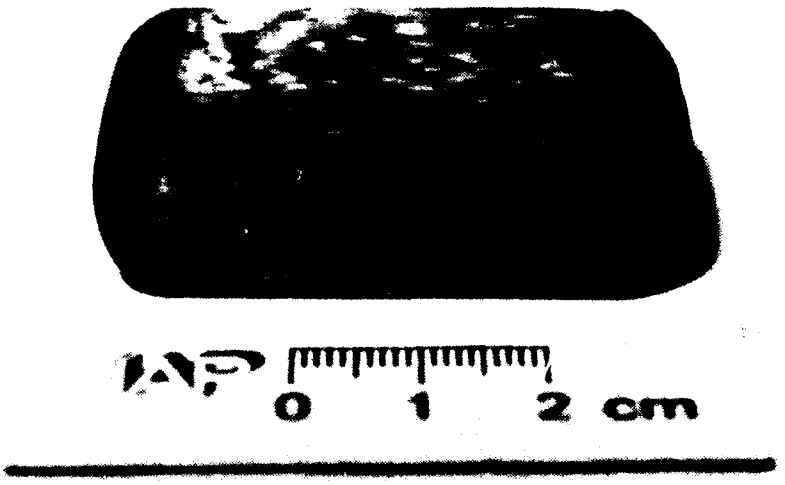

Figure 27. The projectile mass was about 14 g.

4.2 BARREL.

Once we chose the pressure chamber size, we began work on the barrel design. We initially used a vent area to chamber cross section ratio of 0.7. According to our scaling (Figures 20 and 21), this will limit the pressure to 400 MPa at 800 kA. Round rail vents are the easiest to implement. The 0.7 size ratio sets the vent diameter to 6.8 mm. We chose the center to center spacing of the vents to be 11.5 mm, the same as the inner diameter of the pressure chamber. This ensured that the pressure chamber would always be over the equivalent area of one full vent per side.

We used a laminated barrel containment structure in our railgun testing. The laminated structure allows us to design stiff barrels to minimize bore growth. The structure is also easy to assemble and disassemble. We have two standard containment sizes. One is designed for a 15 mm square bore and the other is designed for a 50 mm square bore. While the 15 mm containment fits the bore size better, there were two factors which precluded its use. First, we only had 3 m of the containment structure. We would need about twice that length to achieve the velocity goals of the program. The other disadvantage is that the 15 mm structure is only designed to be used at currents of 500 kA or less. The 50 mm structure is designed to operate at currents up to 1.5 MA. We also had 5.6 m of the larger containment available for testing. We based our barrel design on the 50 mm containment for these reasons.

The bore size, 15 mm by 20 mm, is required to match the projectile. We wanted to maximize the inductance gradient. Table 4 shows how the inductance gradient changes for different sized rails with a 15 mm separation. These values were calculated according to Kerrisk's formula[9]. In the table:

s is the rail separation,

h is the rail height,

w is the rail width, and

L' is the inductance gradient.

Table 4. Inductance Gradient According to Kerrisk.[9]

s (mm)	h (mm)	w (mm)	L' (μH/m)
15.00	19.05	9.52	.4329946
15.00	25.40	6.35	.3865858
15.00	25.40	12.70	.3638727
15.00	25.40	19.05	.3482647
15.00	25.40	25.40	.3365850
15.00	25.40	31.75	.3273745
15.00	31.75	6.35	.3394503
15.00	31.75	9.52	.3298167
15.00	31.75	12.70	.3218635

For a 20 mm bore we need at least a 22 mm rail height. We chose to use standard copper bar stock for rails. This limits us to either 1" or 1.25" rail height. We chose a rail size of 1" by 0.375". This rail size gives us an inductance gradient of 0.374 μH/m. 1" by 0.25" rails would give us a higher L', but would heat up too much during the launch. The 1" by 0.25 " rails would see a temperature rise of about 350 K during a 800 kA launch. The 1" by 0.375" rails would see a temperature rise of only 120K.

In our standard square bore railguns, we use G-10 spacers to support the rails in the containment and maintain proper spacing. The square bores are designed to have a minimum thickness of G-10 and rely on the containment to minimize bore growth.

Since we used the 50 mm containment with a 15 by 20 mm bore, the backing insulators must be very thick. If they were made of G-10, the bore growth would be 0.015". The seals must maintain as close a clearance as possible, so this was unacceptable for the success of the concept. We looked into using advanced ceramics such as Alumina, M/M 400, and M/M 1100. Each of these would limit the bore growth to about 0.004"; however, ceramics tend to break when subjected to a bending stress. Although

the ceramic option is priced competitively, replacement costs and delays would be excessive incase of breakage. The option we chose was a two piece laminated stainless steel spacer, similar in construction to the carrel containment. Venting was provided between the two pieces. G-10 spacers maintain the vent space between the laminated blocks. The laminates reduce eddy current losses in the steel structure. This concept limits the bore growth to 0.001" at 800 kA. Another advantage to this design was that the laminates were easy to replace if necessary.

There is a thin G-10 layer backing insulator between the rails and the backing laminate spacers. The rail spacing insulators are made of G-10. A cross section of the bore is shown in Figure 28. A photograph of a 1 m long section of the barrel is shown in Figure 29.

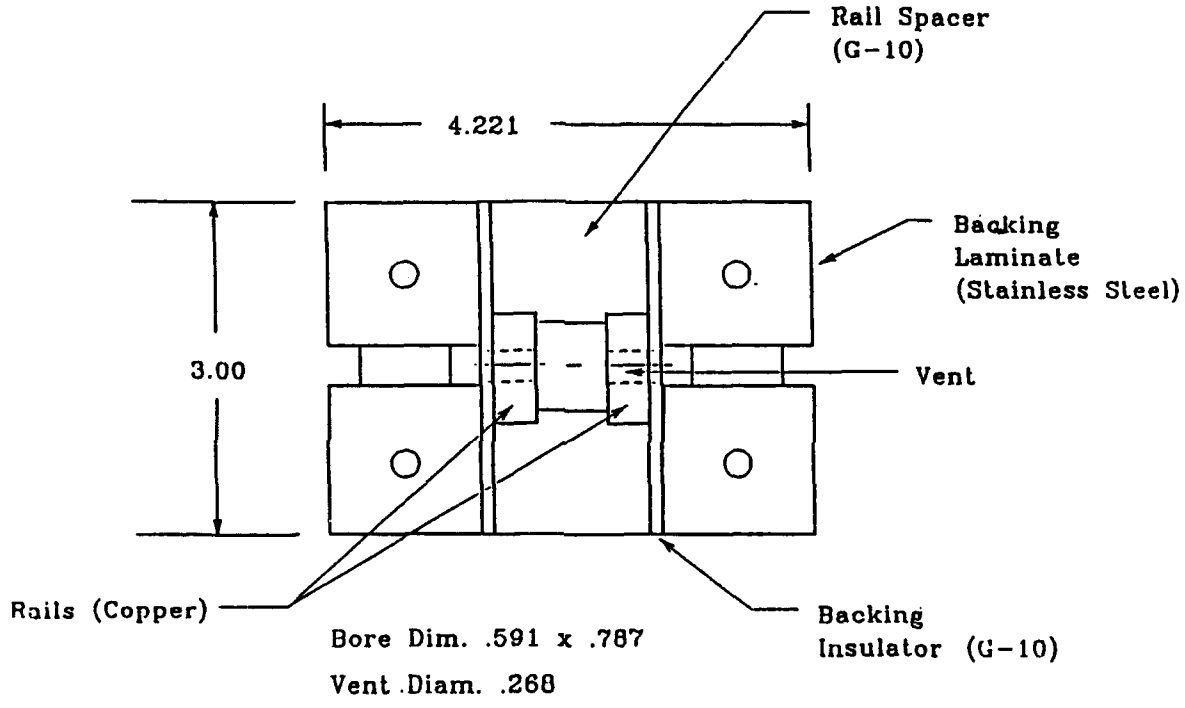

Figure 28. The barrel is designed to minimize bore growth.

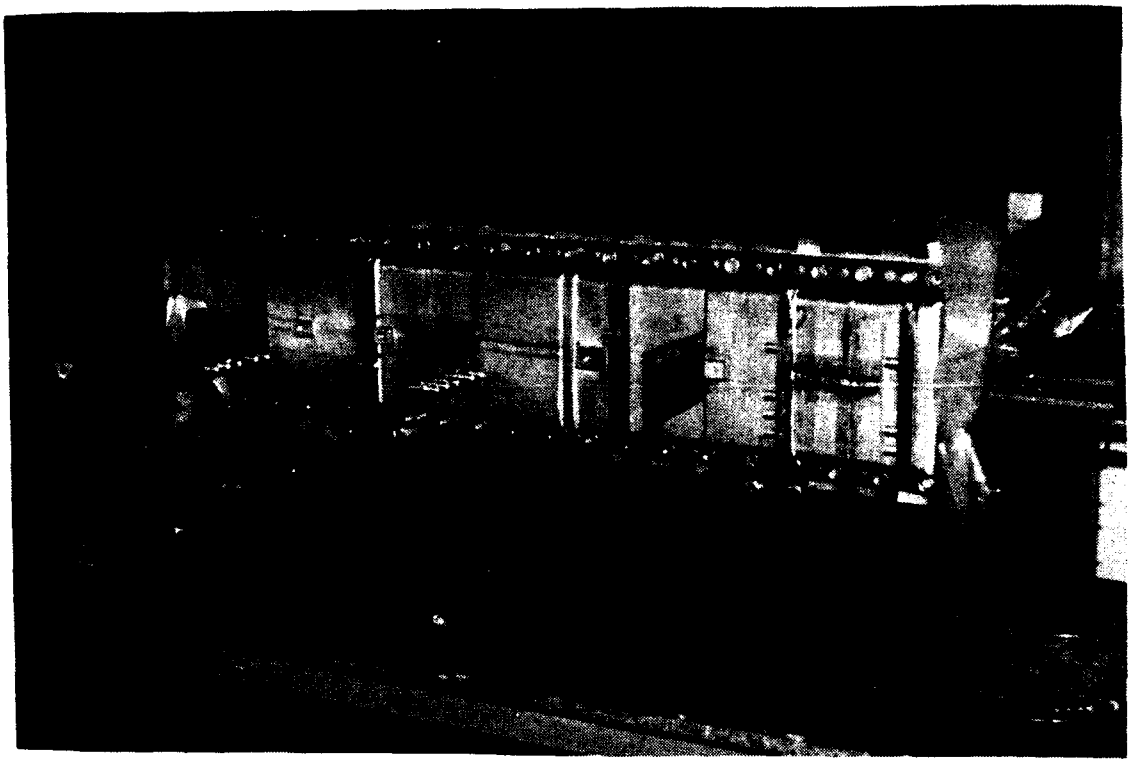

Figure 29. We fabricated the barrel for railgun tests.

4.3 INSTRUMENTATION.

In a railgun test, we measured three quantities: the change in magnetic field with respect to time, muzzle and breech voltage, and current. Each of these quantities can provide valuable insight into the projectile performance and armature behavior. In this section, we will discuss the instrumentation we used to measure these quantities, and the information we can gain from each measurement.

One of the more common measurements made in railgun tests is the change in magnetic field with respect to time, dB/dt, or "B-dot". A probe to measure B-dot is simply a loop of wire oriented normal to the direction of the magnetic field. By Faraday's law, a changing magnetic field will induce a voltage in such a loop. The magnitude of this voltage is equal to the derivative of the total magnetic flux through the loop with respect to time, $d\phi/dt$. If the loop has N turns, this voltage becomes:

$$V_{loop} = N d\phi dt \tag{4}$$

If the dimensions of the loop are small, we can assume that the flux through the loop is uniformly distributed. This means that the flux density in the loop, B, is uniform. The flux in the loop can be written as $\phi = BA$, where A is the area that the loop encloses. Thus the voltage induced around the loop is:

$$V_{loop} = NAdB/dt \quad (5)$$

We refer to such a loop as a B-Dot probe. This probe can be used to monitor the passage of the railgun armature. Since the moving armature produces a change in the magnetic field, the B-Dot probe will register a voltage as the armature passes. A typical signal from a B-Dot probe is shown in Figure 30. Normally, we use this signal to determine the velocity of the projectile by positioning several probes along the length of the rails; however, the B-Dot probe data can also be used to determine the current distribution in the armature. The procedure for doing this is described in the Appendix. This information on the current distribution can tell us how the confined armature is performing. The distribution data will also show if precursor arcs in front of or secondary conduction behind the armature are forming, and thereby indicate if the seals are functioning properly. We used 8-10 B-Dot probes for each test with a 3 m long barrel (less for the shorter barrel).

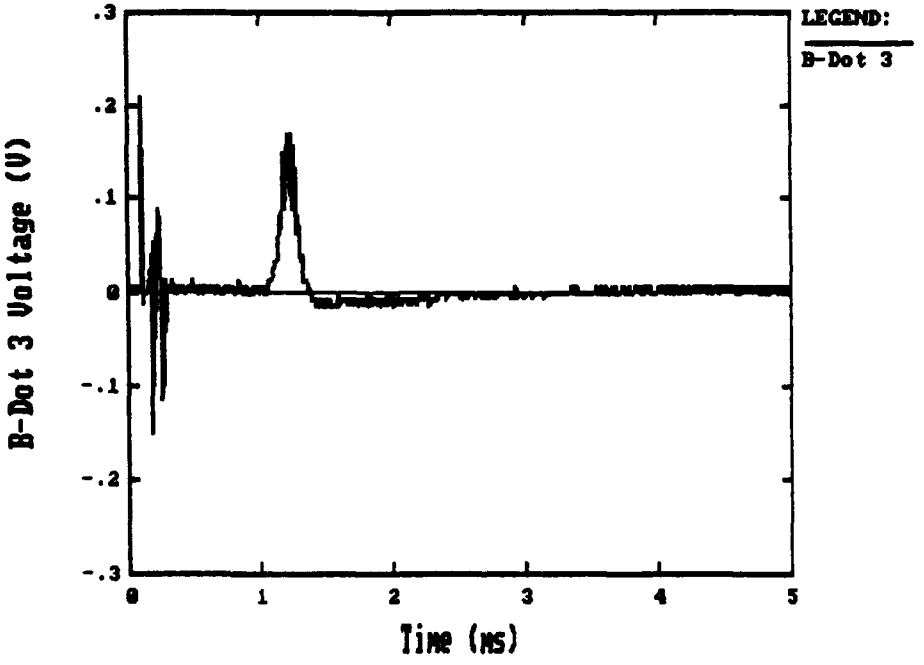

Figure 30. The B-dot probe can detect projectile passage as well as secondary currents.

We also measured the muzzle and breech voltage. We measured these two voltages with the resistor/current transformer technique we used in the static tests. The muzzle voltage is essentially the voltage across the armature. In our tests, the muzzle voltage is a good indication of the condition of the contained plasma. An unconfined plasma armature exhibits a muzzle voltage of 150-300 V, depending on the bore size. A confined plasma armature will exhibit a much higher voltage, typically 500 V or more. An example of the muzzle voltage is shown in Figure 31. The resistance of the confined plasma

armature is substantially higher than that of an unconfined plasma armature mainly due to the smaller conduction area. If the muzzle voltage of a confined armature drops to approximately 200 V, the plasma seals have failed or excessive leakage has occurred, causing a precursor arc in front of the armature, or secondary conduction behind the armature. The breech voltage contains the armature voltage, but the rail resistance and inductance also contribute to the signal.

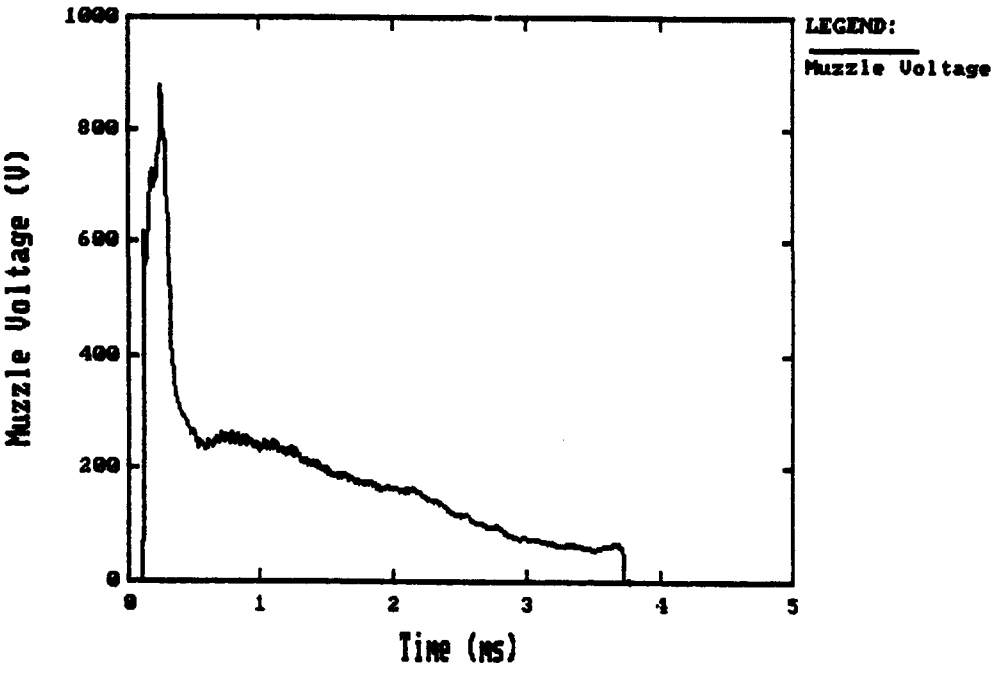

Figure 31. The muzzle voltage is a good indicator of whether or not the armature is confined.

We measured the current in the rails with a calibrated Rogowski coil around one of the rails. A typical current waveform is shown in Figure 32. We need the total current to determine the armature current distribution described above.

By using these three measurements, we were able to diagnose problems with the armatures and improve performance by modifying the projectile on subsequent tests. We describe the railgun tests in the next section.

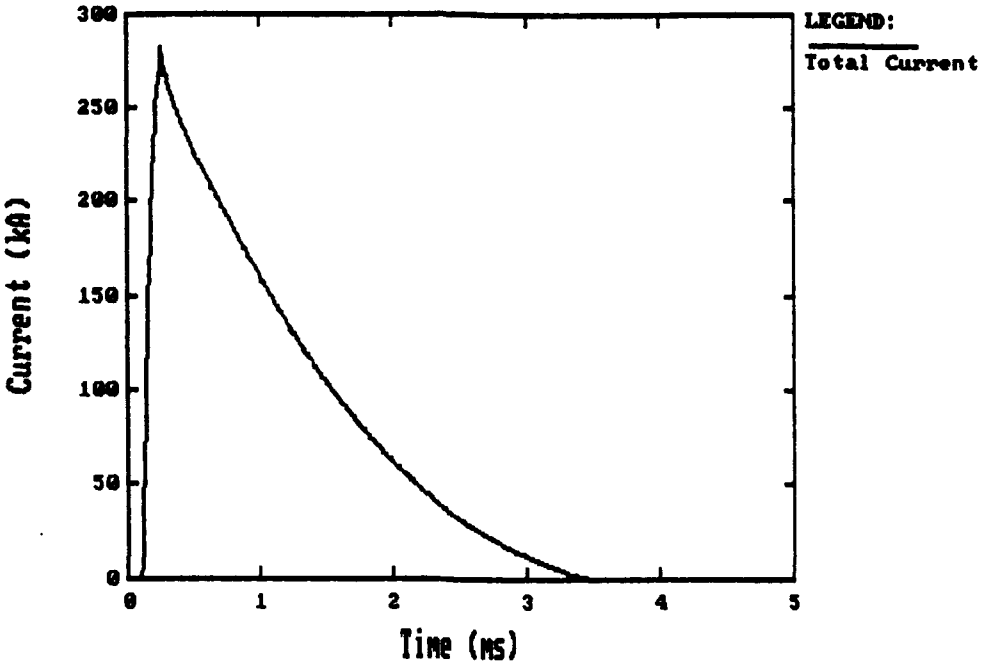

Figure 32. We measure the gun current.

SECTION 5
RAILGUN TESTS

We performed a total of thirteen railgun tests. Seven of these tests were instrument calibration tests. While the current and voltage measurements needed no calibration in situ, the B-Dot probes required calibration each time the gun was disassembled and reassembled. The mutual inductance between the probes and the rails is very sensitive to placement, and for each actual launch, we needed accurate measurements of the mutual inductance of each of the B-Dot probes with the railgun.

The six railgun launches are summarized in Table 5. In each of the launches we modified the projectile design to obtain longer confinement of the armature and better performance. We describe the results of the launches in the following sections.

Table 5. Summary of Phase II Railgun Tests.

Test	Peak Current (kA)	Muzzle Voltage (V)	Initial Condition	Armature Type	Muzzle Velocity (m/s)	Confinement Time*
1	240	600	static start	plasma	280	80 μs
2	280	600	static start	plasma	440	200 μs
3	220	500	injected	plasma	750	400 μs
4	220	300	injected	hybrid	1330	1.0 ms
5	300	480	injected	hybrid	1800	1.4 ms
6	300	480	injected	hybrid	1500	1.1 ms

* Confinement time is duration - high muzzle voltage was sustained.

5.1 TEST 1.

In our first test, the peak current was 240 kA. We launched the projectile from a static start. The barrel length was 1 m. The projectile mass was 14.8 g. We loaded the projectile into the barrel from the breech of the gun. We sized the projectile to have a slight interference fit (0.0015") from rail to rail, to obtain an effective seal. The vent diameter was 6.8 mm for the first two launches. This gives a total vent area to chamber cross section ratio of 0.7.

In the first test, shown in Figure 33, the high initial muzzle voltage (>600 V) indicates that the armature is well confined for about 80 μs. The voltage then decays to about 200 V. We believe that the

seal failed and a precursor arc formed. The muzzle voltage probe was destroyed at 1.1 ms, after the precursor arc exited the muzzle. The breech voltage in Figure 34 showed that 200 V was maintained between the rails until current decayed to near zero.

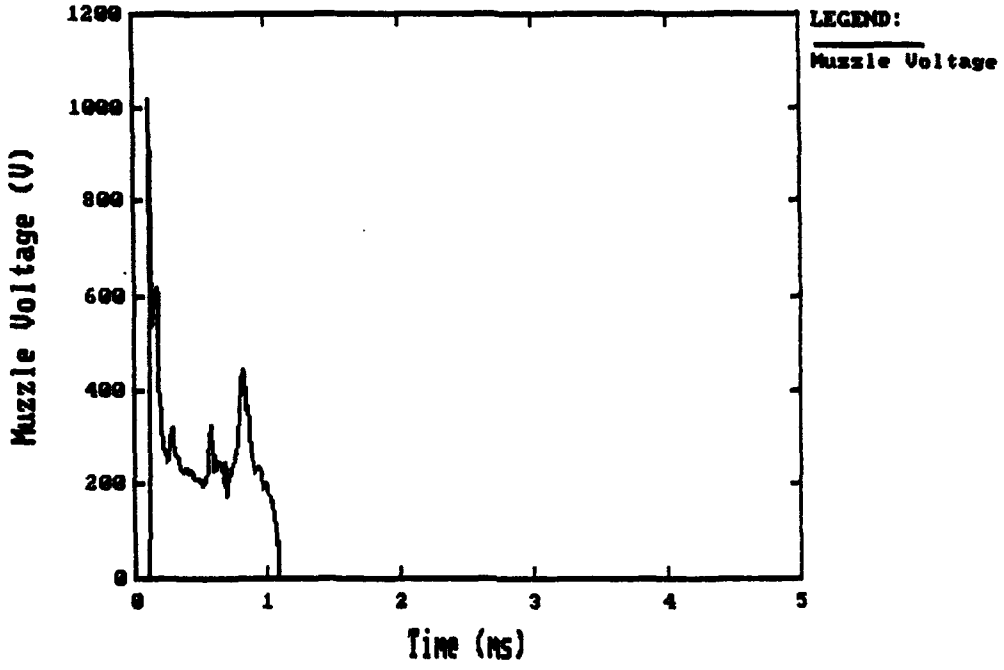

Figure 33. The armature in Test 1 was confined for 80 μs.

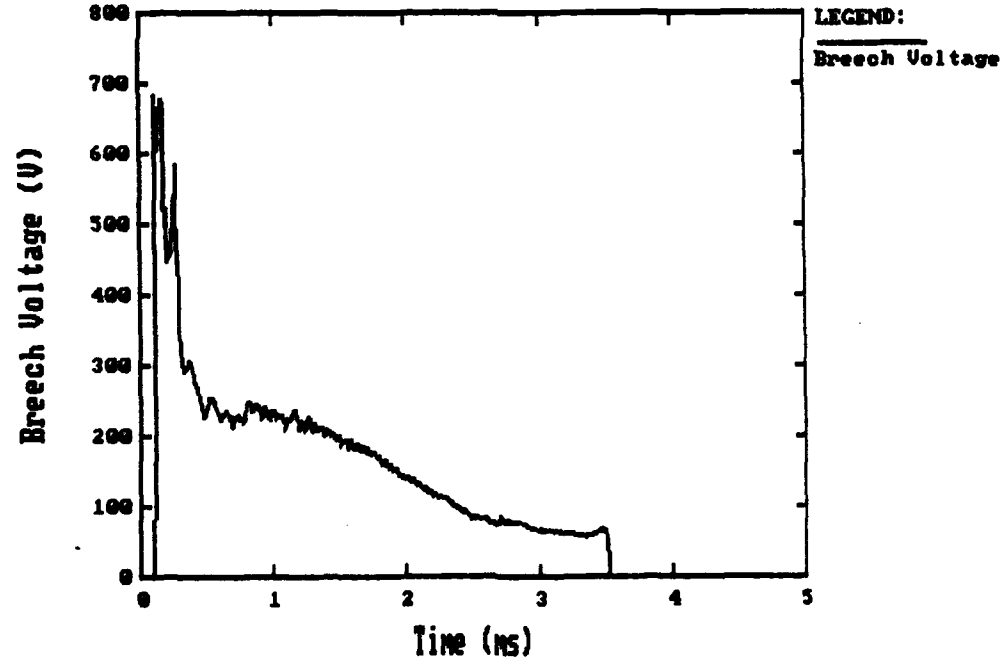

Figure 34. The breech voltage showed the armature condition after the muzzle probe was destroyed.

Analysis of the B-Dot data indicated that a precursor arc formed at 240 μs. It achieved a velocity of over 3 km/s before slowing down near the muzzle. The signal from the third B-Dot is shown in Figure 35. This probe was located 0.264 m from the breech of the gun. The first spike at 250 μs is a precursor arc travelling past the probe. The small negative spike at 800 μs is the precursor exiting the muzzle. The small "hump" in the B-Dot signal at 1.7 ms is the projectile going past the probe. Another probe at 0.705 m from the breech shows only the precursor arc. This means that current ran out before the projectile passed that position. This is consistent with the damage on the rails. We saw rail damage from the plasma armature until a little over 0.5 m from the breech. The precursor arc caused little damage to the rails because of its high velocity. The projectile did not achieve any significant velocity before current ran out. We recovered the projectile intact.

One of the prominent features of this launch was that the rails were severely eroded around the projectile starting position. This is typical of plasma armatures launched from a standing start. In this case, however, this erosion causes excessive leakage around the front and rear seals. This leads to both precursor arcs and secondary currents behind the projectile. Most of the current in this launch went into the precursor arc after the seal failed.

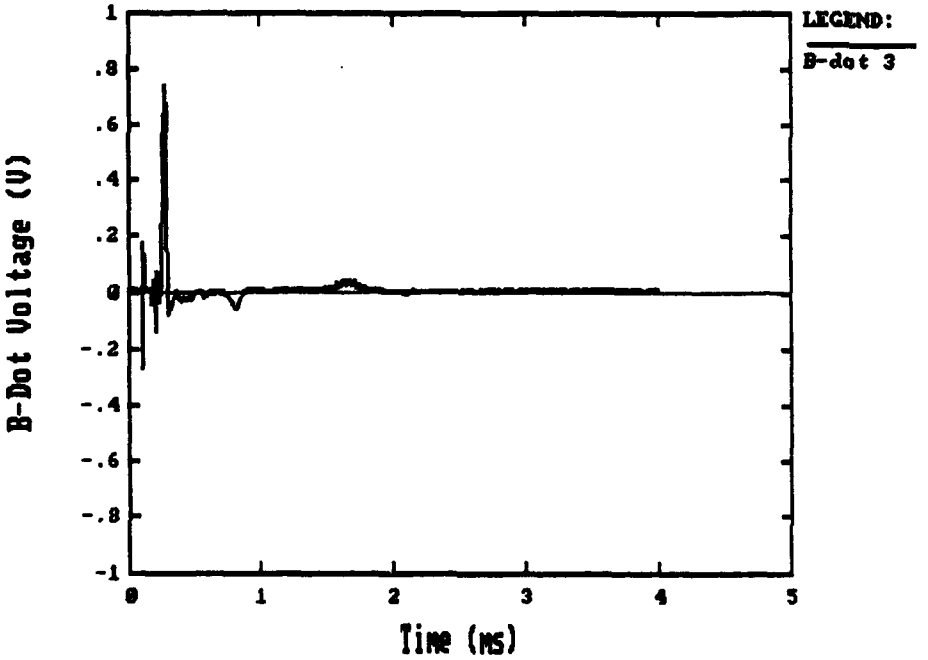

Figure 35. There was a precursor arc in front of the armature.

5.2 TEST 2.

The projectile in our second launch was identical to the first. The peak current was 280 kA. The muzzle voltage was over 600 V for 200 μs. Its peak value was over 800 V. This is shown in Figure 36.

The projectile mass was 14.5 g. The projectile reached 440 m/s before current ran out. The B-Dot data again showed that the current ran out before the projectile reached 0.706 m. A typical B-Dot signal from this test is shown in Figure 37. The noise at the beginning is a small precursor arc. In this test, the projectile passage is much more distinct than in the first launch. The precursor arc did not affect the acceleration of the projectile significantly.

The static start of the armature eroded the rails severely at the beginning of the launch as in the first test. The erosion again caused excessive leakage at least in front of the confined armature, which caused a precursor arc to form. The B-Dot data also showed that the armature was longer than the projectile. This indicated that secondary current was flowing behind the projectile. This was also caused by rail erosion while the projectile was still stationary. The remainder of our launches were injected into the railgun before current initiation. This reduced the rail erosion caused by static start.

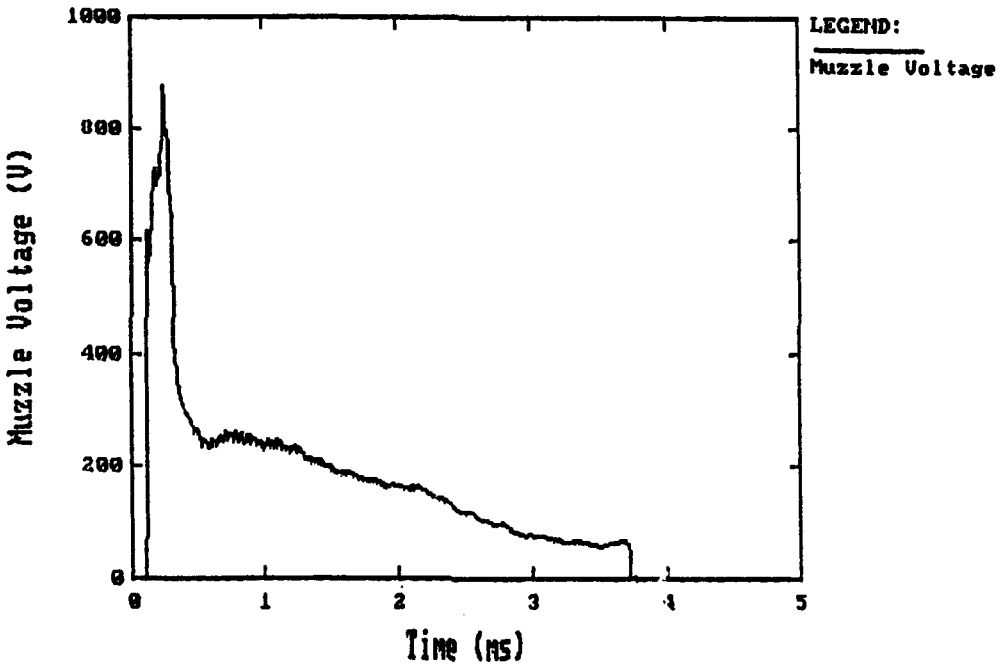

Figure 36. The armature was confined for about 200 μs.

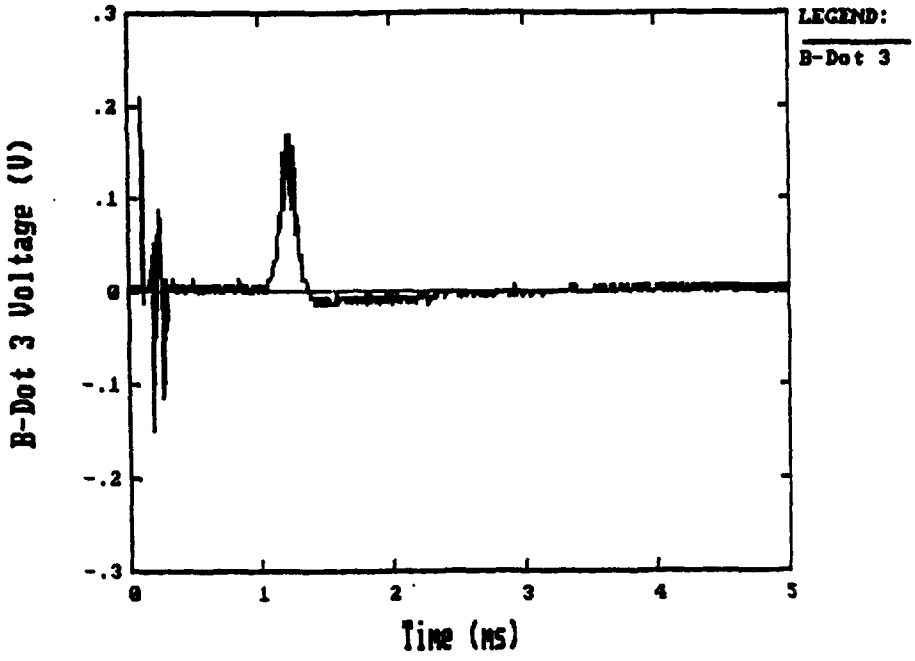

Figure 37. The B-dots showed a small precursor arc.

5.3 TEST 8.

For the remainder of the tests, we used a barrel 3 m long. We accelerated the projectile into the railgun with a compressed gas injector. In our first launch with the injector, the interface between the power supply and the railgun arced due to the high voltage of the confined armature. We repaired the interface, but the problem of high armature voltage remained. A low leak rate is critical to the success of the armature concept. With the high voltage, even small leaks are sufficient to cause precursors and secondary currents. We decided that we needed to take steps to reduce the rail to rail voltage of the confined plasma armature.

To reduce the rail-to-rail voltage, we focussed on reducing the armature resistance. The first approach we took was to increase the pressure inside the containment chamber. For the remaining tests we used a rail vent diameter of 4.8 mm. This decreased the vent area to chamber cross section ratio to 0.35. This reduction in vent size increased the pressure and hence increased the conductivity of the plasma somewhat.

We added an additional groove to both the front and the rear seals. The assembled projectile is shown in Figure 27. The peak current was 220 kA. This test generated a significant precursor arc. Only one of the B-Dot probes detected the projectile passage.

Most of the current was in the precursor. The muzzle voltage is shown in Figure 38. The muzzle voltage was still about 500 V. This was only slightly lower than the voltage we saw in the launches from

a static start. The rails showed that the armature initiated just inside the gun structure. However, there was only evidence of confinement for about 400 μs. The well defined damage tracks from the confined plasma were only 3-4" long. We saw light arc erosion from the precursor down the entire length of the gun. The muzzle voltage drops from 600 V to 300 V at 2.2 ms. This coincides with the precursor (and projectile) passing the first B-Dot position. The projectile carried only a small fraction of the current after the precursor separated from the main armature. This is shown by the current distribution in Figure 39. The precursor carries about 90% of the current. The precursor exited the bore at about 2.5 ms. This is indicated in the muzzle voltage signal by a sudden increase in voltage.

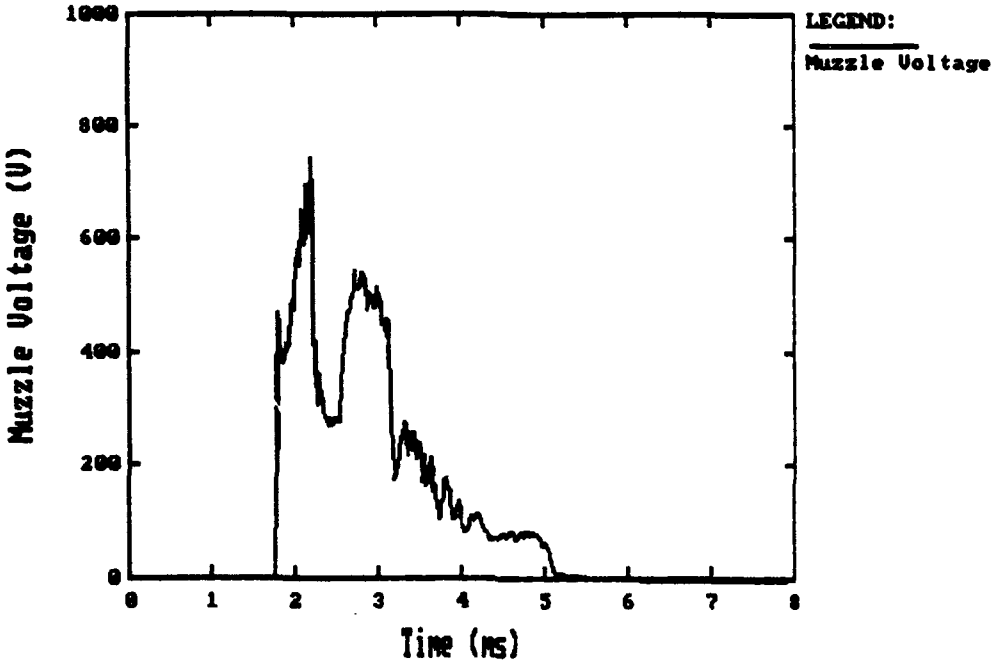

Figure 38. The armature was confined for about 400 μs.

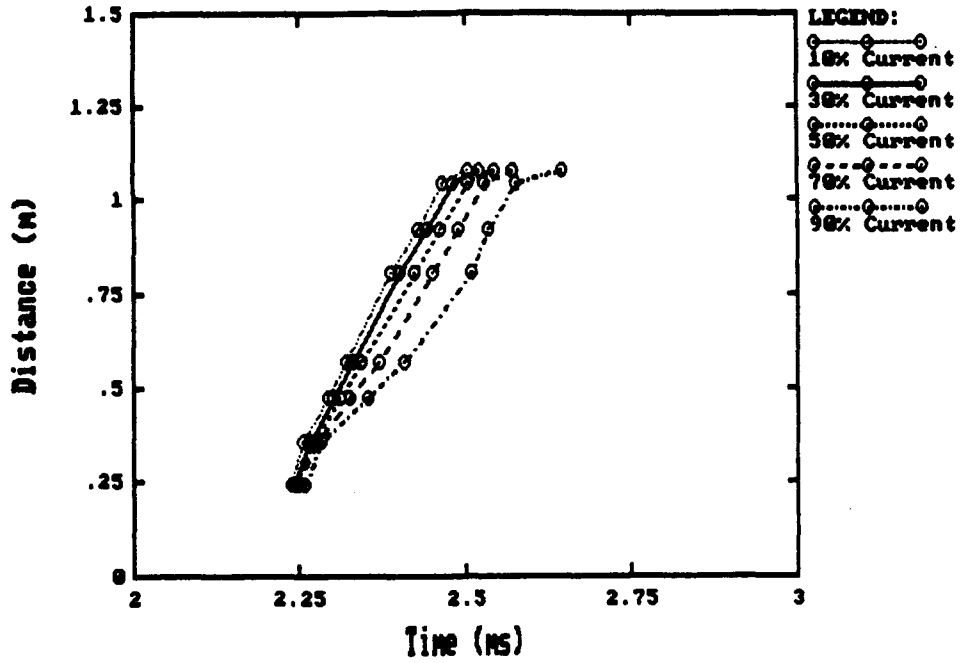

Figure 39. The precursor carries 90% of the current.

There was still a small amount of current flowing through the armature after the precursor broke away. As the precursor exited the bore, the remaining current diverted back into the armature. We recovered the projectile with only slight damage. The most significant damage was to the containment chamber itself. In this design, the ends of the chamber rode on the rail surface and were not supported by the seal structure. We found that one end of the chamber was sheared off even with the bottom of the seal groove. This caused excessive leakage and the high current precursor. This was also our first indication that the graphite composite was beginning to deteriorate.

5.4 TEST 10.

We performed this launch under the same conditions as the previous one. The only difference was that this armature was a hybrid armature. The projectile had an aluminum cylinder fit into the containment chamber. Our idea was to reduce the armature voltage eliminating the column voltage drop of the plasma armature. The penalty for this approach is that the projectile mass was increased. The mass of the projectile was 18 g. We also adjusted the seal design so that a seal blade would rest against the containment chamber and support the edges riding on the rails.

The muzzle voltage for this launch is shown in Figure 40. It showed a low voltage armature for the entire launch. The ramp shape at the beginning of the pulse is similar to that of a forward vented hybrid armature. The drop in voltage at 3 ms means that a precursor has formed. This is supported by the B-Dot data. The current distribution for the test, shown in Figure 41. The 10% and 30% contours split indicating the formation of a precursor. The main armature continued, but the armature lengthened. The projectile was not recovered intact, but the B-Dot data and the rails indicated that the seal on one side

of containment chamber failed. The narrow damage track on the other rail indicated that the seal on the other rail functioned well.

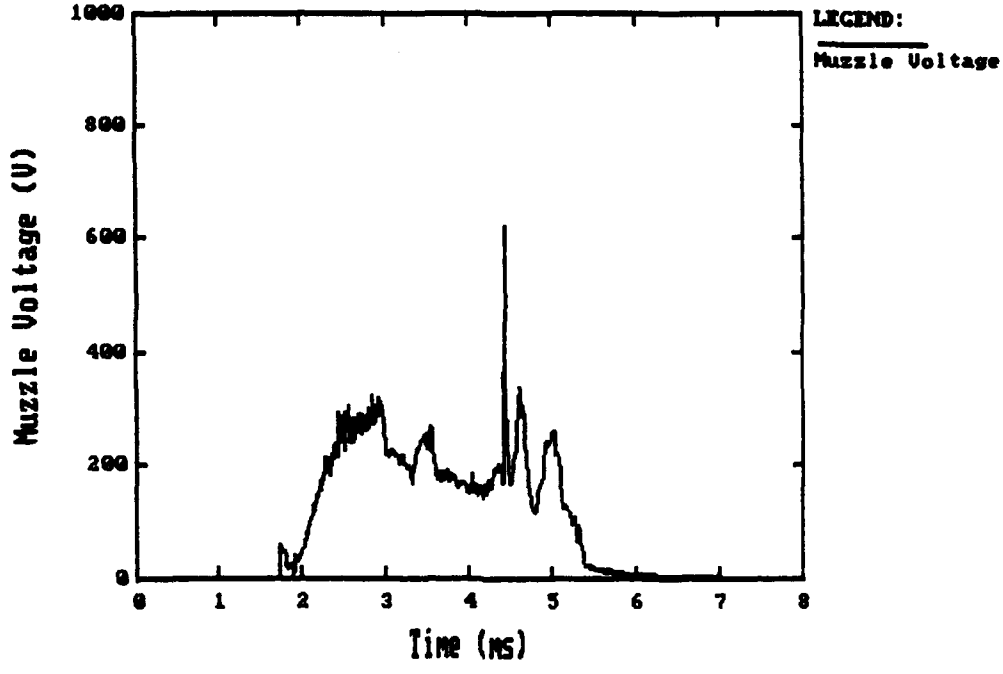

Figure 40. The confined hybrid armature shows a lower initial voltage than a plasma.

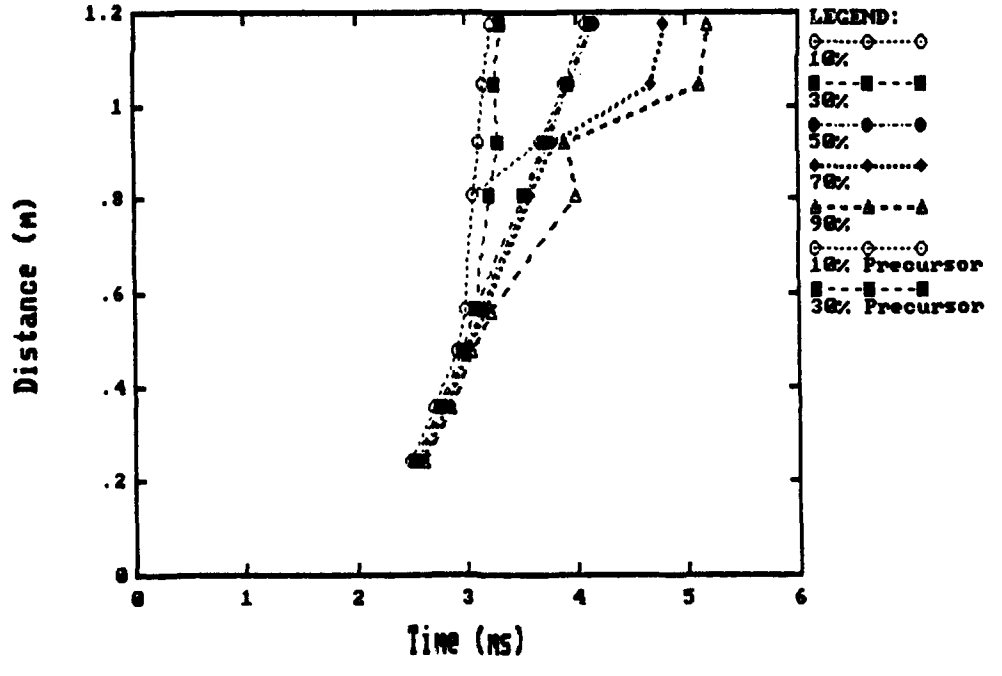

Figure 41. A precursor arc formed at 3 ms.

In this launch there was more evidence that the graphite was deteriorating. This is normally due to the introduction of moisture into the epoxy of the composite. We built two test pieces to find out how serious the problem was. Both test pieces started to delaminate (peel) soon after the curing process was complete. We bought new graphite to build the remaining projectiles.

5.5 TEST 11.

We modified the projectile design again after Test 10. We eliminated the groove next to the containment chamber by filling it with epoxy. This gave the containment edge additional structural support. We also used new graphite to fabricate the projectile. The peak current was 300 kA. The muzzle voltage is shown in Figure 42. Again, the ramp shape was present. During this test, the armature was confined for about 1.4 ms. The current distribution is shown in Figure 43. At about 3.4 ms, a precursor arc formed in front of the armature. This is indicated by the 10%, 30%, and 50% contours in the distribution. These contours accelerate and stay compact. The main armature indicated by the 70% and 90% contours slows down and lengthens. This indicated that a precursor of at least 50% of the current separated from the armature. The lengthening of the main armature indicated that secondary currents were also present.

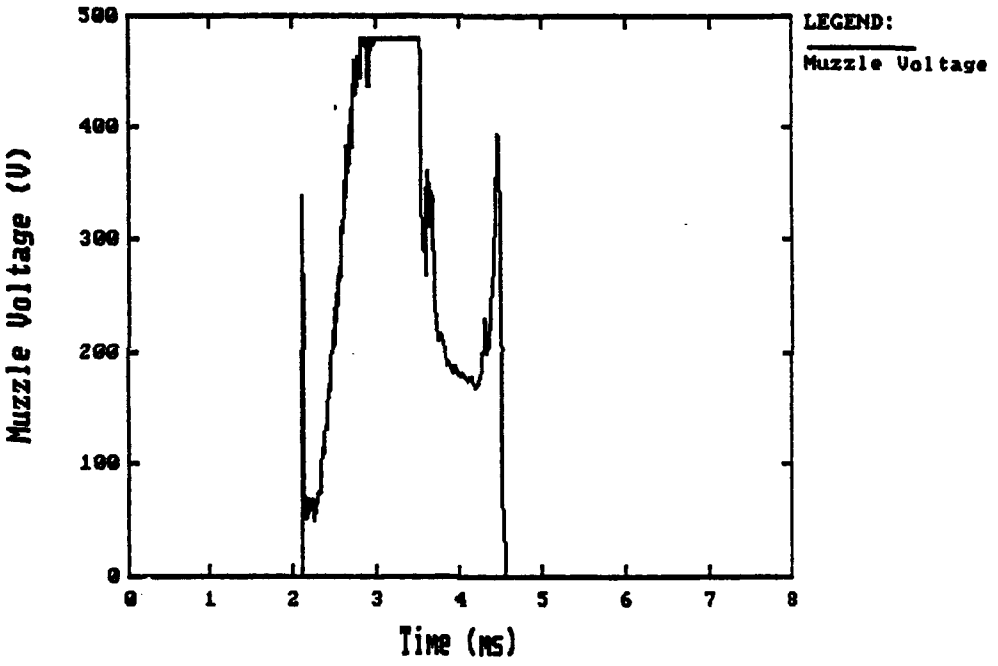

Figure 42. This armature was confined for 1.4 ms.

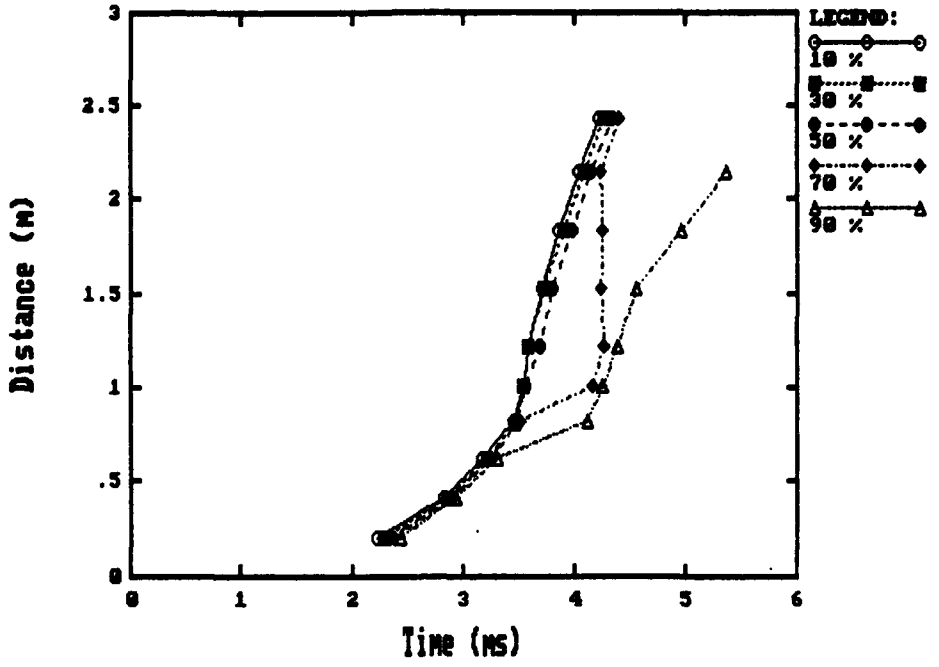

Figure 43. A precursor arc formed at 3.4 ms.

5.6 TEST 13.

We used the same projectile design as in the previous test except that the epoxy filled grooves were omitted. By leaving the material intact, instead of machining grooves then filling them with epoxy, we felt that we could improve the strength of the containment edge and achieve better sealing. The conditions were the same as in the previous launch. The peak current was 300 kA. The muzzle voltage is shown in Figure 44. This showed that the armature was contained for about 1.1 ms. This was confirmed by the current distribution shown in Figure 45. Most of the current went into a precursor at about 3.2 ms. The main armature again had secondary currents behind it.

The slight reduction in confinement time may indicate that the epoxy may help the seal. The epoxy we used is more compliant than the G-10 in the seal structure. This may have helped the filled grooves act as rail following blades of the seal, dynamically minimizing the seal to rail clearance and making a better seal. We will discuss our conclusions in the last section.

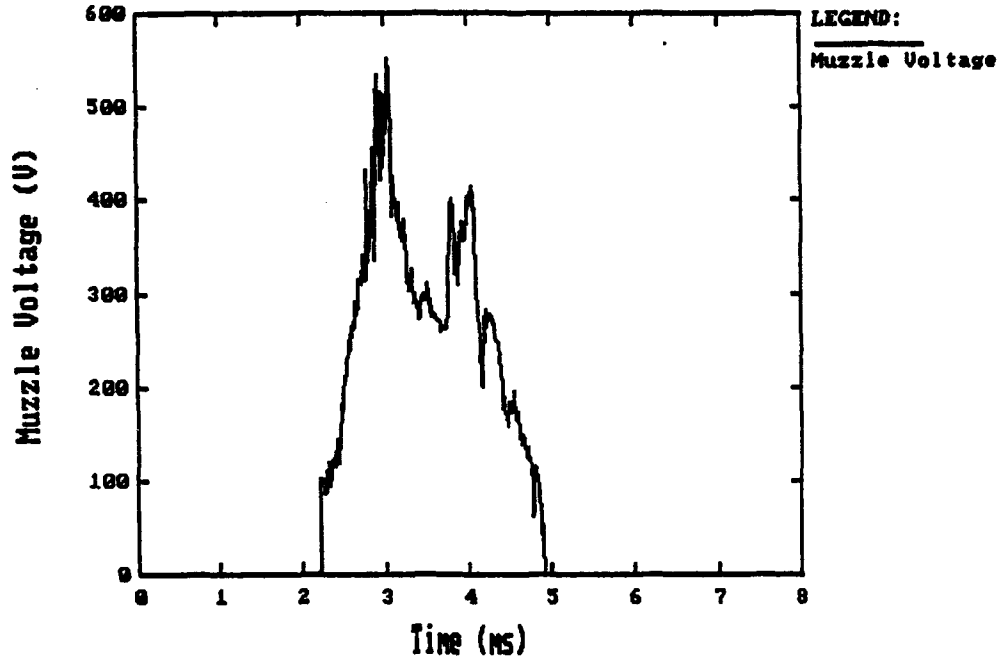

Figure 44. The armature was confined for 1.1 ms.

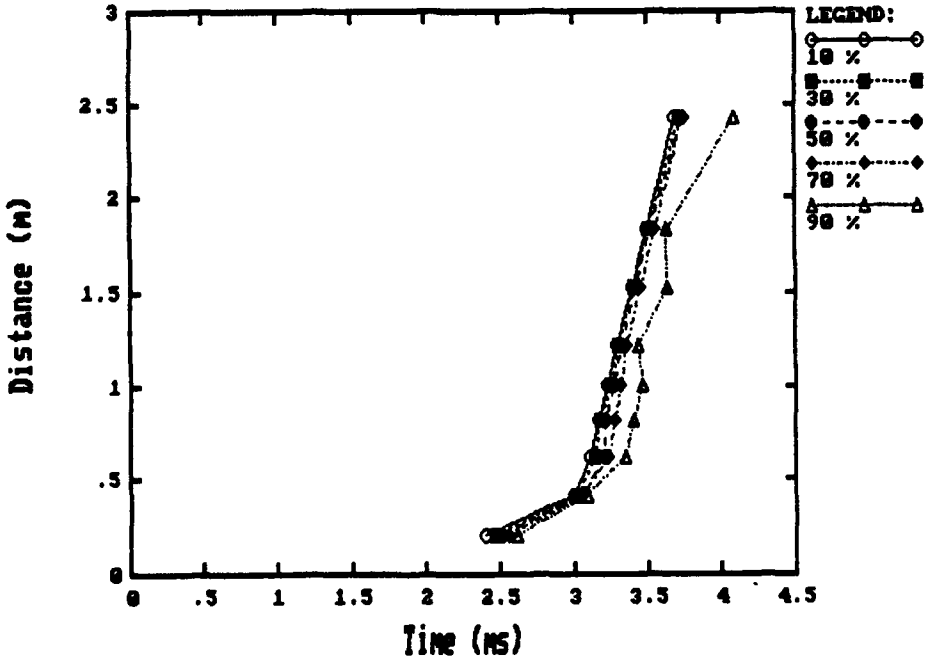

Figure 45. Most of the current went into a precursor at 3.2 ms.

SECTION 6

INTERPRETATIONS AND CONCLUSIONS

Our railgun tests showed that we were making progress toward proving the confined, vented armature concept could exceed the velocity limit; however, the seals in front of and behind the armature are still a problem. The seals must be more effective in eliminating plasma from the bore during the entire launch, and not just a small portion of it.

We reviewed our design to see what design changes were necessary for further improvement. We believe that the labyrinth seal is still the most promising seal concept for the confined armature, but there are several difficulties in the design which could be addressed in future improvements.

First, in our implementation of the labyrinth seal, we suspect that leakage around the top and bottom (near the bore insulator surfaces) of the projectile to be the main problem. Our design can only use the edge of the plasma containment to prevent leakage between the top and bottom of the projectile and the bore insulators. The close fit we used for the projectile dimension from insulator to insulator was not sufficient to prevent leakage along the insulator.

The second problem with the design was the issue of maintaining the dynamic clearance of the seal along the rails throughout the launch. The clearance must be minimized for the seal to be effective. There are several factors that make this a difficult problem. First, the vent holes in the rails make the rail surface rough. At higher velocities it is difficult for the seal to maintain contact with such a surface. Another factor is bore growth. The same magnetic forces accelerating the projectile down the bore are simultaneously pushing the rails apart. This may cause the seal to fail if bore deflection is too great. We believe that our barrel design was stiff enough for this not to be a problem in our design, but further improvements are possible.

Variations in the bore dimensions can also affect the dynamic clearance of the seals. Inherent variations in bore dimensions caused by machining and assembly can be a problem, as well as variations caused by ablation of rail material by the armature can cause the dynamic seal clearance to grow to levels where excessive plasma leakage will occur. Of these two causes, rail ablation is the least controllable.

The dynamic clearance of the seal is also adversely affected by erosion and abrasion of the seal material as it travels along the bore. This problem only gets worse at higher velocities.

One problem inherent in the concept is that the high voltage between the rails is made worse by confining the armature. The confined armature has a smaller cross sectional area than a normal armature, hence a higher resistance. The higher voltage makes the acceptable seal leakage lower, so the seal must

be better or the voltage must be reduced.

We feel that we can design a projectile that solves the problems we have enumerated. One such concept is shown in Figure 46. We can entirely surround the pressure containment with a circular labyrinth seal (two blades and one groove). We can incorporate this into our present design by slightly narrowing the graphite overwrap in the rail-to-rail direction, and placing a glass fiber wound tube inside the graphite pressure tube. The glass fiber tube and the graphite tube form the first labyrinth (blade and groove) of the seal (a complete circle around the containment). A second labyrinth can be made in the glass fiber body, similar to our present design. The difference is that this second blade and groove extend the full rail height, to eliminate leakage at the corners. The seals are symmetric about the pressure chamber, and will allow the same leakage to the font and back. This will allow precursors to be eliminated as effectively as secondary currents behind the armature. We could also incorporate a compliant material into some seal surfaces to improve tracking of the rail, and maintain the minimum dynamic clearance. The projectile dimensions are such that no modifications are needed to the barrel. We estimate that the mass of this design will be 11 g.

We simulated railgun launch performance with this design. Figure 47 shows the simulated current profile for our power supply. The current is held essentially constant at ~330 kA for about 2.5 ms. Figures 48 and 49 shows the position and velocity data versus time, respectively for a gun length of 8 m. The projectile can exceed 5 km/s if the armature is contained for 3 ms. We believe that the proposed design can improve the containment time from the demonstrated 1.4 ms to the required 3 ms.

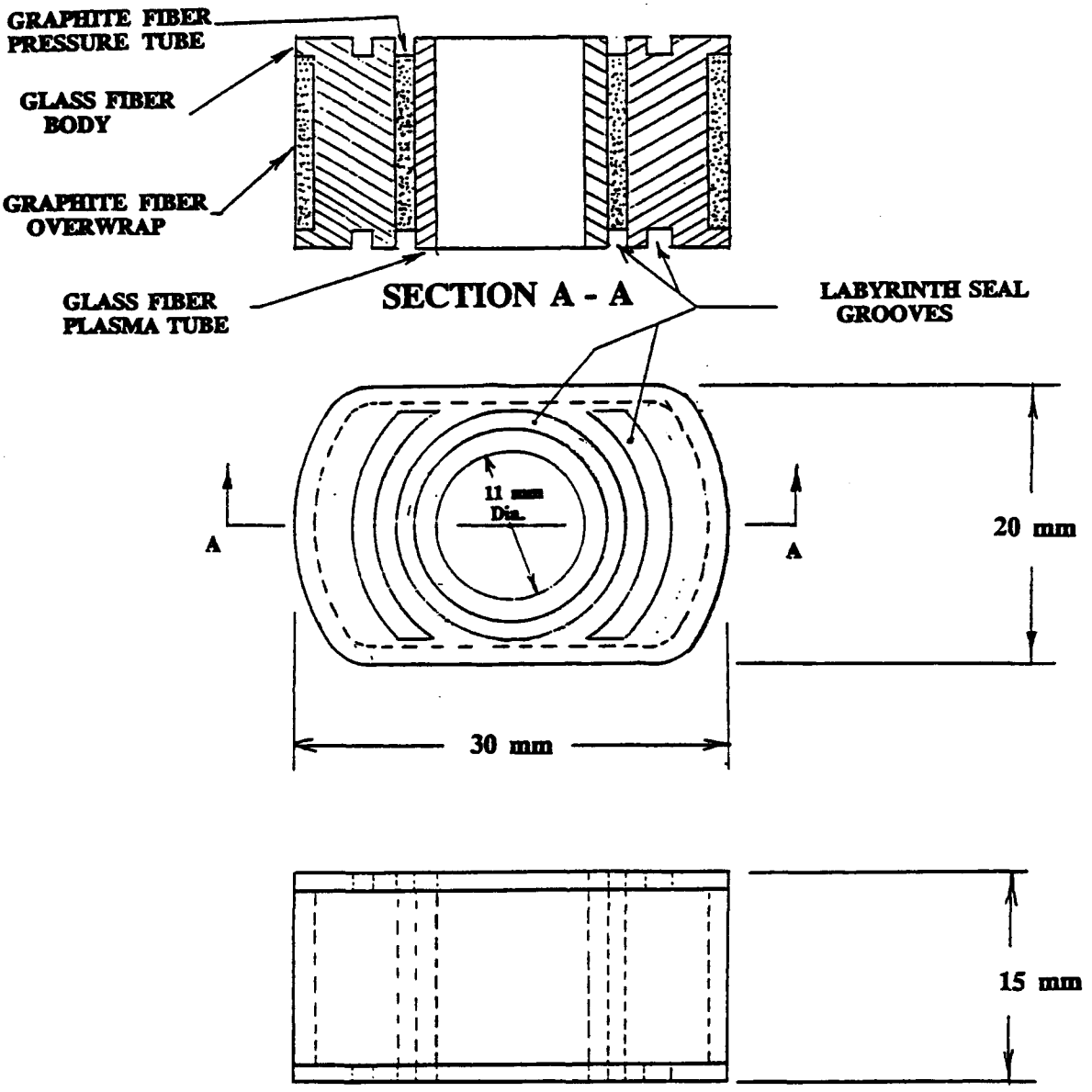

Figure 46. We can modify the seal design for better function.

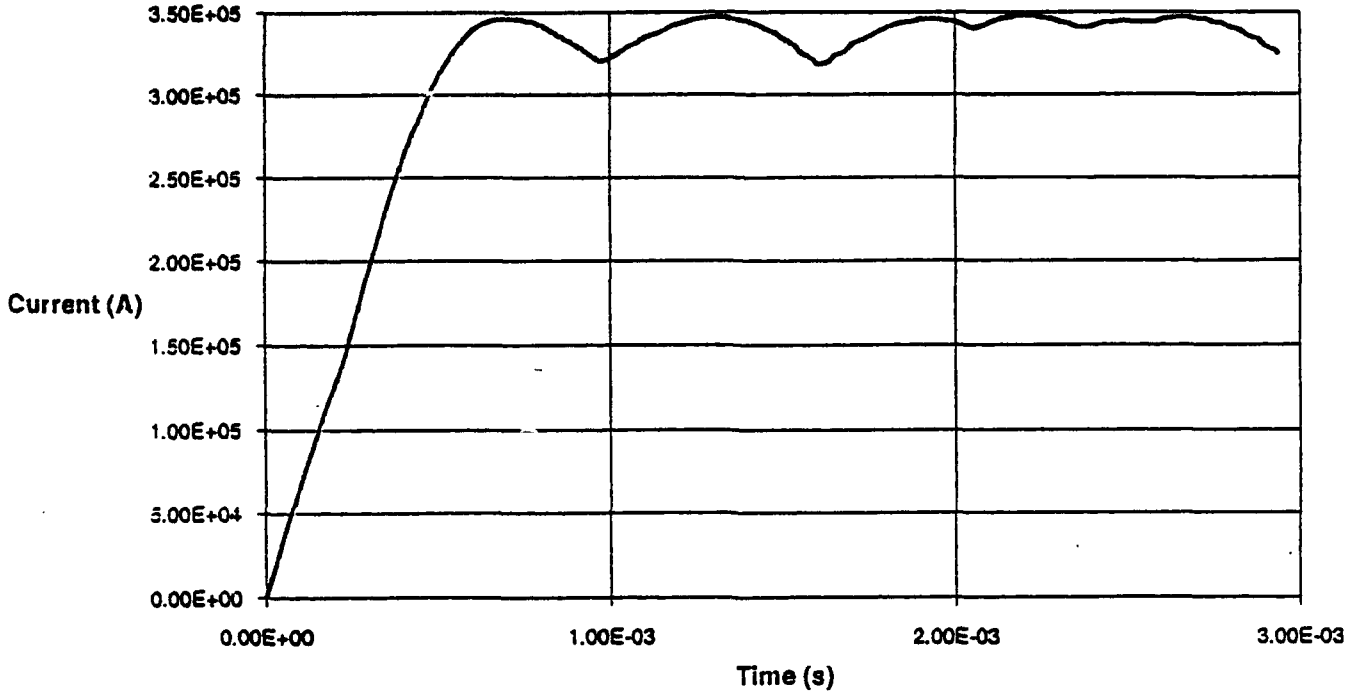

Figure 47. We need 330 kA for almost 3 ms to achieve 5 km/s.

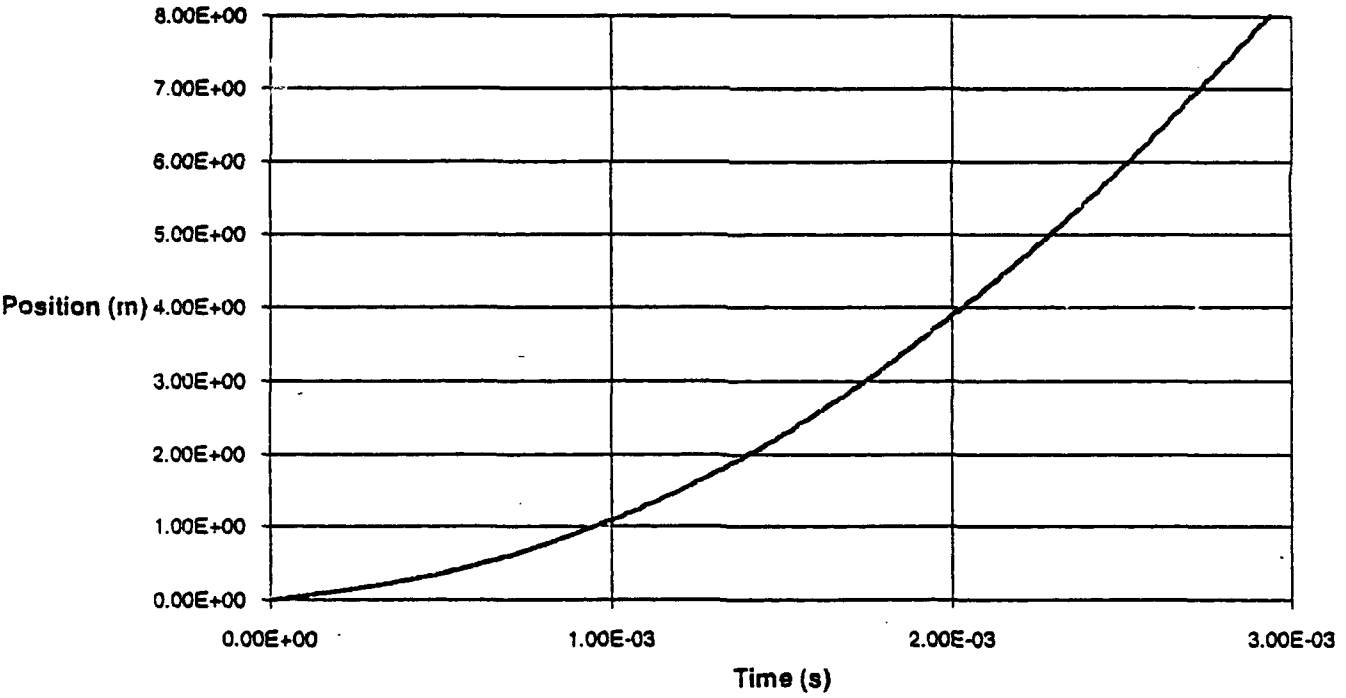

Figure 48. We simulated a railgun launch for the proposed projectile and an 8 m gun.

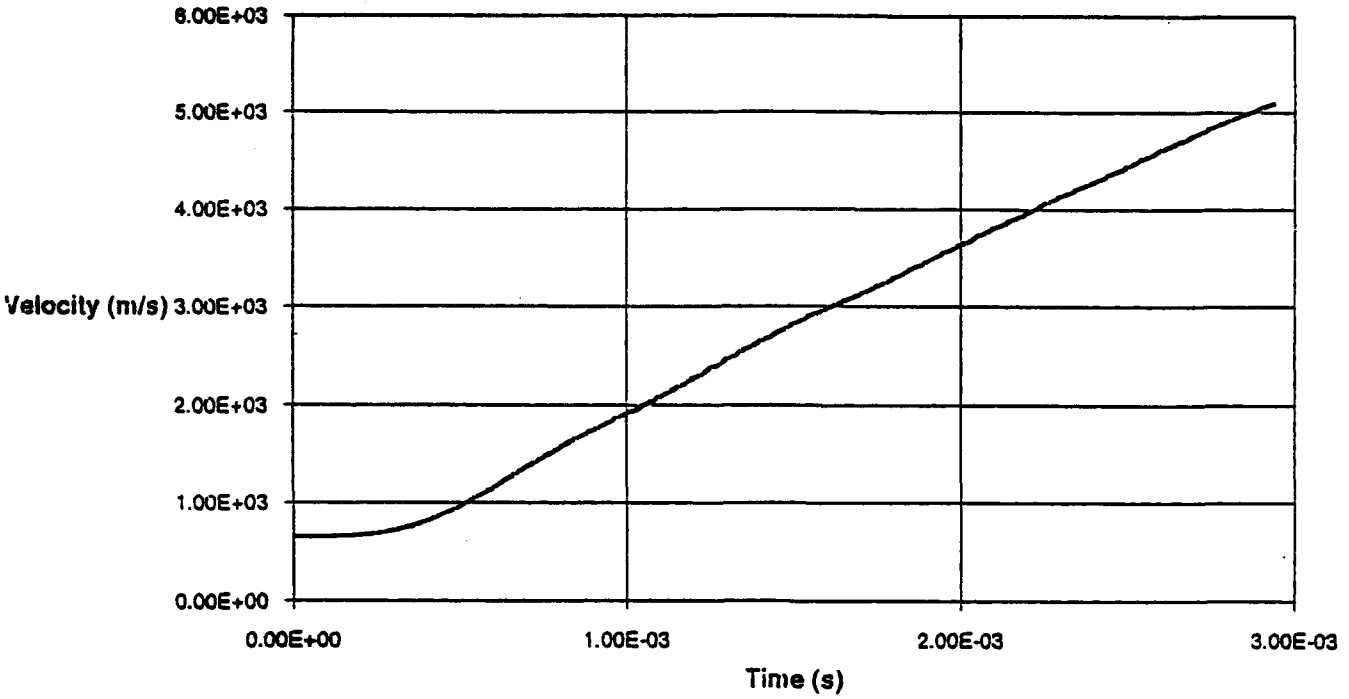

Figure 49. The 11 g projectile will reach 5 km/s.

SECTION 7

LIST OF REFERENCES

1. Barber, J.P., and Marshall, R.A., IEEE Transaction of Magnetics, VOL. MAG-27, NO. 1, p.323.
2. Bauer, D.P., and Knoth, E.A., IAP Proposal for Nested Chevron Gun for Ultra High Launch Velocities, IAP-PR-89-36.
3. Maas, B.L., IAP Proposal for Hypervelocity Launcher for Aerothermodynamic Experiments, IAP-PR-91-08.
4. Parker, J., IEEE Transaction on Magnetics, VOL. MAG-25, NO.1, p. 418.
5. Juston, J.M., Barber, J.P., and Challita, A., Phase I Final Report (Contract # DNA-TR-89-114).
6. Juston, J.M., Barber, J.P., and Challita, A., IAP Proposal for Railgun Armature Velocity Improvement - SBIR Phase I, IAP-PR_87-41.
7. Marshall, R.A., "The Properties of Copper and Hydrogen Plasmas", Wollongong, NSW 2500, Australia, September 1986.
8. Peickii and Christiansen, Product Engineering, 20 March 1961, p. 57.
9. Kerrisk, J.F., "Current Distribution and Inductance Calculations for Railgun Conductors", LA-9092-MS US-34, Nov., 1981, Los Alamos National Laboratory.

APPENDIX

OBTAINING THE ARMATURE CURRENT DISTRIBUTION FROM B-DOT DATA

The armature current distribution is an important indication of armature performance. In our application, we need to know what the length of the armature is, and whether alternate current paths have formed in front of or behind the armature. For the confined armature to function properly, the main armature must be the axial length of the confinement chamber (within the accuracy of the measurements). A longer armature indicates that the armature is not functioning as designed. Small precursor arcs are acceptable; however, secondary current behind the main armature is detrimental to armature performance. Likewise, precursor arcs containing more than about 30% of the total current detract from armature acceleration. Hence, we need a method to determine the current distribution in the armature to monitor the armature performance, and diagnose deviations from anticipated results. The following is a description of a method to determine the armature current distribution from existing B-Dot data.

We designed our B-Dot probes to measure the changes in the rail current. Therefore, they will pick up not only the passing armature, but also any alternate current paths as they move down the rails. A typical B-Dot signal is shown in Figure 50. The voltage signal is proportional to the change in the magnetic field at the probe position. This means that the signal is proportional to di/dt at the probe position. The proportionality constant is simply the mutual inductance between the probe and the rails. We measure the mutual inductance by fixing a short between the rails at the muzzle, and driving current through the gun. The mutual inductance is simply the B-Dot signal level divided by the di/dt in the gun (alternately, integrate the B-Dot signal, and divide by the gun current). We can perform this division as well as the data manipulations mentioned below with our data analysis software, CAMNEW, and any graph plotting software.

During a railgun test, we determine the current distribution at each B-Dot location by using the mutual inductance and the following technique. We take the B-Dot signal, such as that shown in Figure 50 and integrate it. The result is shown in Figure 51. We then divide the integrated signal by the mutual inductance of the probe. The result is the current in the rail which has passed the probe position. An example of this rail current is shown in Figure 52. We normalize the rail current to the total current in the gun by dividing the rail current by the gun current. The normalized current is shown in Figure 53. For each probe, there is a similar normalized current profile. We replot the normalized data from all the probes as shown in Figure 54. The "contours" of constant normalized current indicate how current travels down the rails. For a metal or confined armature, the armature is short. Short, compact armatures are indicated on the plot by "contours" that stay close together. In a normal plasma or hybrid armature, the contours spread out, indicating that the armature is lengthening. This means that secondary

current conduction is affecting the armature performance. A short, compact armature indicates that most of the accelerating force is being exerted on the projectile.

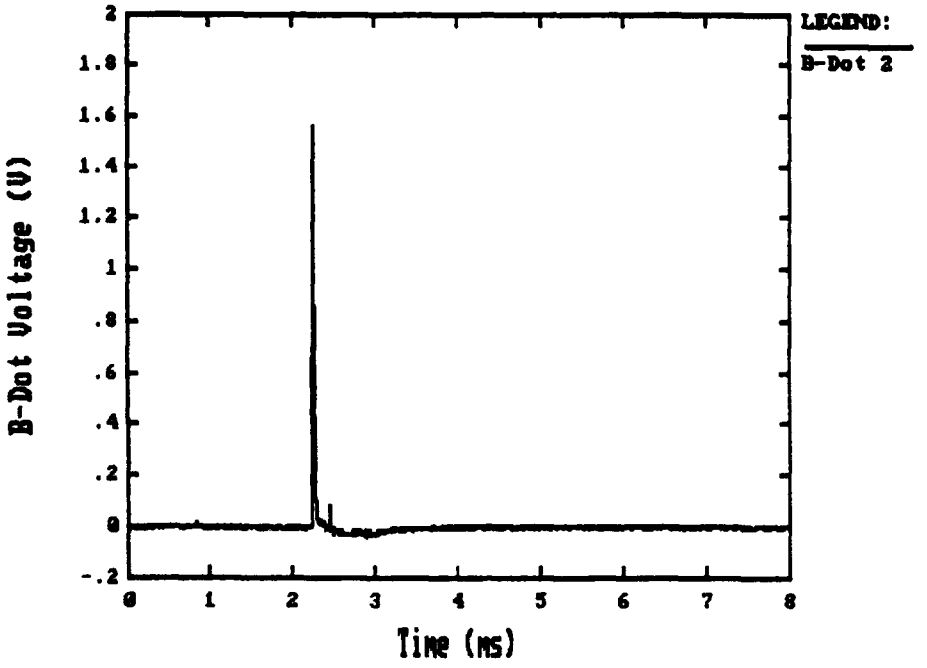

Figure 50. We measure dB/dt at several positions along the board. This B-dot signal is typical of those in Test 8.

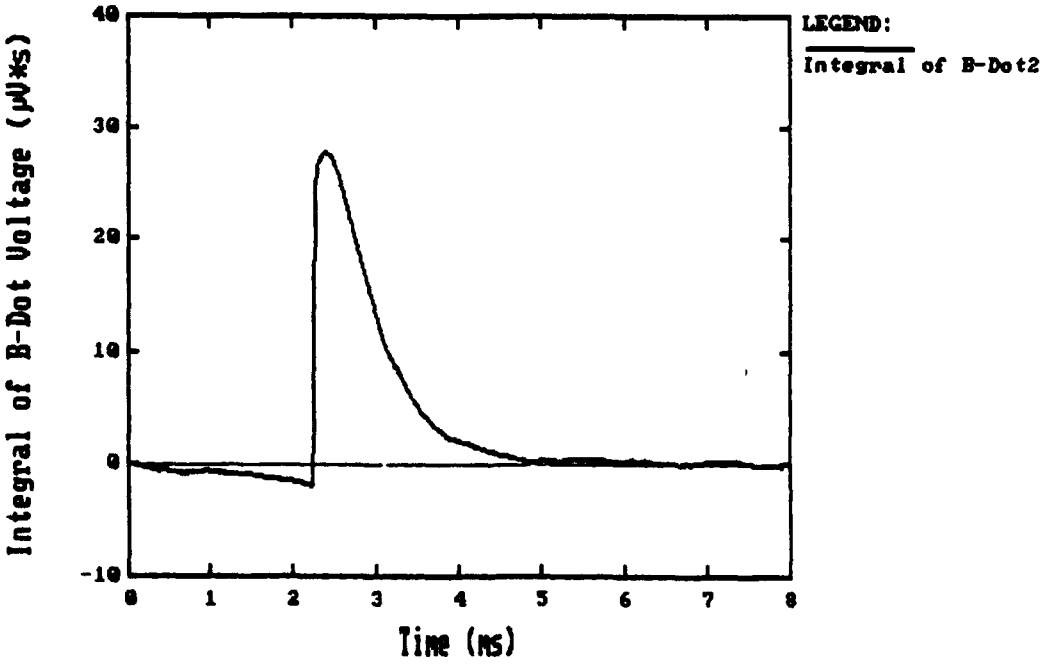

Figure 51. The integrated B-dot signal is proportional to the rail current that has passed the probe position.

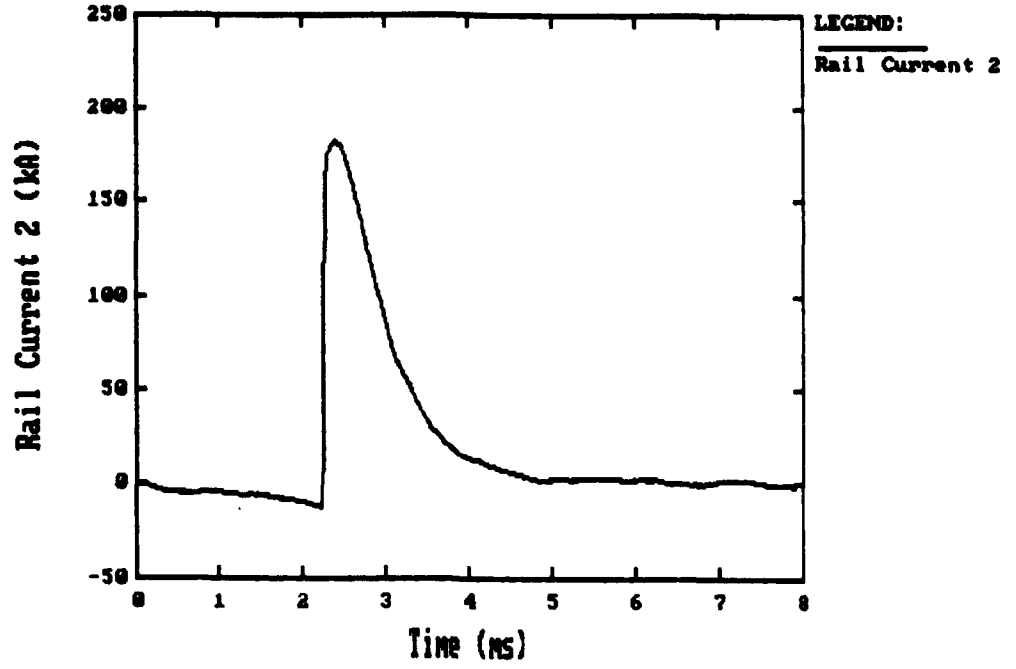

Figure 52. We divide the integrated B-dot signal by the mutual inductance to get the rail current.

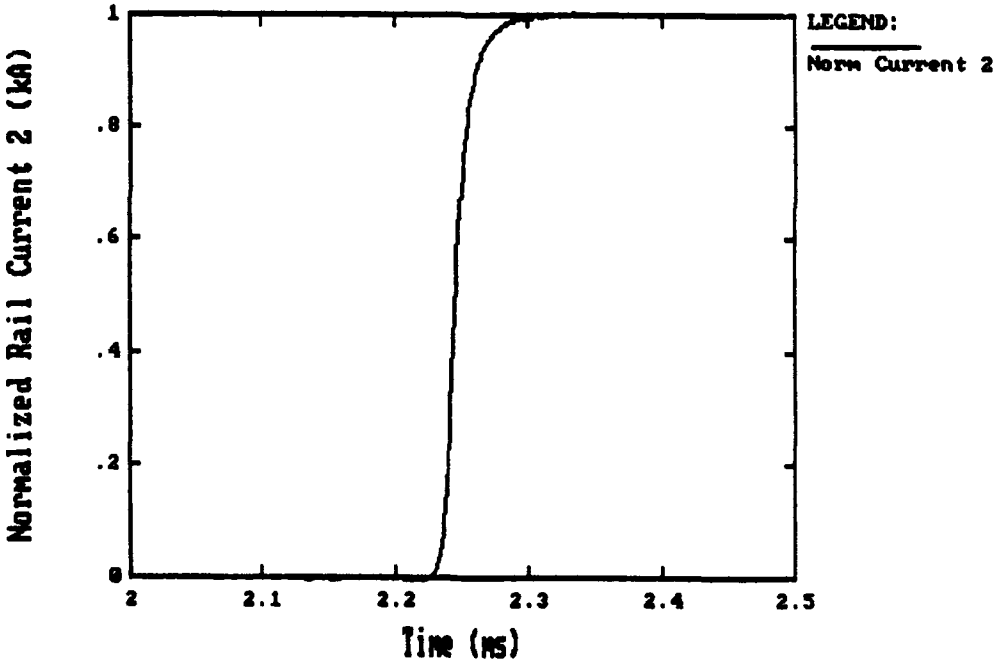

Figure 53. We divide the rail current by the total gun current to normalize the current at the probe position.

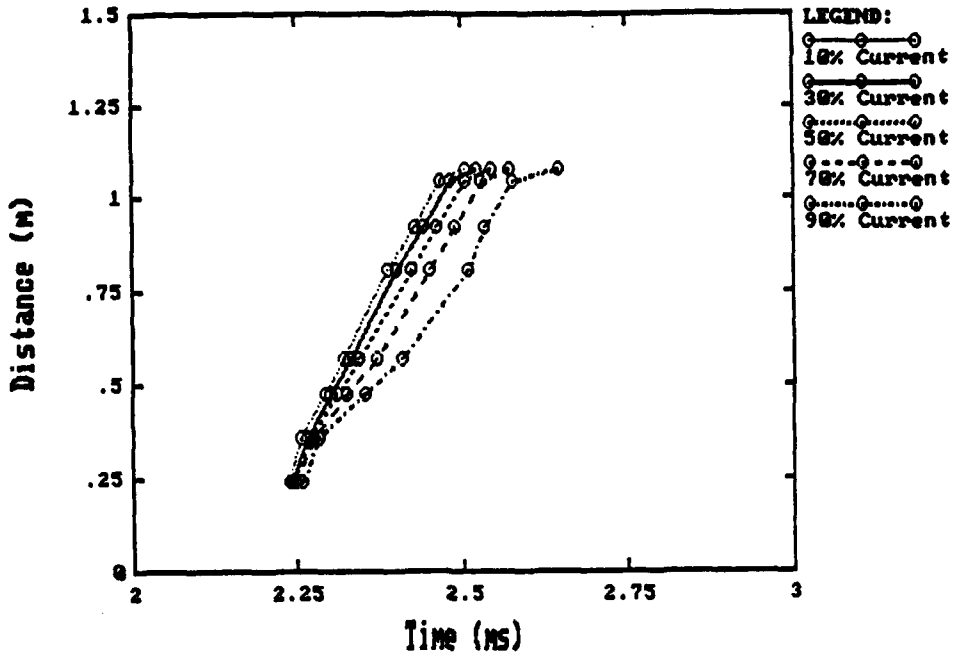

Figure 54. **We replot the normalized current data to show current distribution in the gun.**

DISTRIBUTION LIST

DNA-TR-92-10

DEPARTMENT OF DEFENSE

ASSISTANT TO THE SECRETARY OF DEFENSE
ATTN: C NELSON
ATTN: LT COL P RUSTAN
ATTN: MIL APPL COL HEUBUSCH, USAF
ATTN: TNS

DEFENSE ADVANCED RSCH PROJ AGENCY
ATTN: LTC J BENO
ATTN: PETER KEMMY
ATTN: TTO

DEFENSE NUCLEAR AGENCY
ATTN: DFPR
ATTN: DFRA
ATTN: DFSP
ATTN: DIRECTOR
ATTN: OTA
2 CYS ATTN: TITL

DEFENSE TECHNICAL INFORMATION CENTER
ATTN: DTIC/FDAB

DEPARTMENT OF THE ARMY

U S ARMY BALLISTIC RESEARCH LAB
ATTN: SLCBR-IB-M

U S ARMY FOREIGN SCIENCE & TECH CTR
ATTN: SCOTT LEBEAU

U S ARMY STRATEGIC DEFENSE CMD
ATTN: CSSD-AT-P

U S ARMY AREDC
ATTN: THADDEUS GORA/SMCAR-FSC

DEPARTMENT OF THE NAVY

NAVAL RESEARCH LABORATORY
ATTN: CODE 4775/R FORD

DEPARTMENT OF ENERGY

LAWRENCE LIVERMORE NATIONAL LAB
ATTN: RONALD HAWKE

LOS ALAMOS NATIONAL LABORATORY
ATTN: JERALD PARKER

SANDIA NATIONAL LABORATORIES
ATTN: ORG 1220 MAYNARD COWAN

DEPARTMENT OF DEFENSE CONTRACTORS

EML RESEARCH INC
ATTN: RONALD GELLATLY

IAP RESEARCH INC
2 CYS ATTN: D P BAUER
2 CYS ATTN: L E THURMOND

KAMAN SCIENCES CORP
ATTN: D ELDER

KAMAN SCIENCES CORP
ATTN: DASIAC

KAMAN SCIENCES CORPORATION
ATTN: DASIAC

MAXWELL LABS
ATTN: DR I MCNAB

PHYSICS INTERNATIONAL CO
ATTN: C STALLINGS

SCIENCE APPLICATIONS INTL CORP
ATTN: KEITH JAMISON

TEXAS, UNIVERSITY AT AUSTIN
ATTN: WILLIAM F WELDON

WESTINGHOUSE ELECTRIC CORP
ATTN: J FLETCHER

WESTINGHOUSE STC
ATTN: DANIEL DEIS